END
DATE
FILMED
8 82
DTIC

SECURITY CLASSIFICATION OF THIS PAGE *(When Data Entered)*

REPORT DOCUMENTATION PAGE		READ INSTRUCTIONS BEFORE COMPLETING FORM
1. REPORT NUMBER AFOSR-TR- 82-0572	2. GOVT ACCESSION NO.	3. RECIPIENT'S CATALOG NUMBER
4. TITLE *(and Subtitle)* STUDIES OF BISTABLE OPTICAL DEVICES		5. TYPE OF REPORT & PERIOD COVERED FINAL Sept. 1978-Jan.1982
		6. PERFORMING ORG. REPORT NUMBER
7. AUTHOR(s) Elsa Garmire		8. CONTRACT OR GRANT NUMBER(s) AFOSR-78-3686
9. PERFORMING ORGANIZATION NAME AND ADDRESS Center for Laser Studies University of Southern California Los Angeles, CA 90007		10. PROGRAM ELEMENT, PROJECT, TASK AREA & WORK UNIT NUMBERS 61102F 2305/B2
11. CONTROLLING OFFICE NAME AND ADDRESS AFOSR/NE Building 410 Bolling AFB, DC 20332		12. REPORT DATE May 15, 1982
		13. NUMBER OF PAGES 81
14. MONITORING AGENCY NAME & ADDRESS*(if different from Controlling Office)*		15. SECURITY CLASS. *(of this report)* UNCLASSIFIED
		15a. DECLASSIFICATION/DOWNGRADING SCHEDULE

16. DISTRIBUTION STATEMENT *(of this Report)*

Approved for Public Release;   Distribution Unlimited

17. DISTRIBUTION STATEMENT *(of the abstract entered in Block 20, if different from Report)*

DTIC
ELECTE
AUG 3 1982
H

18. SUPPLEMENTARY NOTES

19. KEY WORDS *(Continue on reverse side if necessary and identify by block number)*

Bistable Optical Devices   Optical Signal Processing
Nonlinear Fabry-Perot
Optical switches
Image Processing
Electro-Optic modulators

20. ABSTRACT *(Continue on reverse side if necessary and identify by block number)*

This report outlines the results of a three-and-a-half year
research program in Optical Bistability and its applications for
Optical Signal and Image processing. The results of the program
are in four areas: 1. Study of image processing in the ultra-
thin nonlinear Fabry-Perot, and demonstration (theoretically)
that parallel processing of more than 10^9 bits in 10^{-9} seconds
is feasible with current technology. This is an overall bit rate
of 10^{15} per second, using bistability in InSb.

DD FORM 1 JAN 73 1473

SECURITY CLASSIFICATION OF THIS PAGE *(When Data Entered)*

#20. 2. Study of hybrid electro-optic bistable devices for array processing, and development of a concept to simultaneously process over 2500 parallel bits in a nanosecond, in a linear array. 3. Studies of bistability in new materials and new geometries. This includes saturable absorbers, InAs, distributed feedback and four-wave mixing. 4. Studies of dynamic effects in optical bistability, including critical slowing down, pulse shaping, overshoot switching, alternate switching risetime detection, pulse detection, and self-oscillation.

Accession For

NTIS GRA&I
DTIC TAB
Unannounced
Justification

By
Distribution/

Availability Codes

| | Avail and/or |
| Dist | Special |

A

DTIC
COPY
INSPECTED

TABLE OF CONTENTS

I. SUMMARY OF RESULTS AND INTRODUCTION TO BISTABLE DEVICES

A. Summary

The bistable optical device (BOD) is a generic name for a class of nonlinear optical processors which use feedback and optical nonlinearities to achieve a nonlinear transfer curve which may be used to optically process information. The transfer curve (light output as a function of light input) of these devices may be nonlinear, monostable, bistable, multistable, self-pulsing, or chaotic, depending on the characteristics of the system. One direction of this research has been to understand and clarify the regimes of operation, in order to develop useful nonlinear optical processors.

Most research to date has emphasized single element bistable devices. However, the bistable optical device shows promise for image processing by using ultra-thin Fabry-Perots, as will be described. The ultimate realization of image processing depends on obtaining low power levels for bistability, in order to obtain a large number of resolvable spots. We have investigated both new materials and new geometries for use in bistable optical devices with a view toward achieving high speed image processing. We will show that there are image processing and linear array processing geometries for which the bistable optical device holds much promise in optical signal processing.

The first of our studies described in this report is an investigation of the number of resolvable spots which can be expected from bistable devices which have been demonstrated to date. We show in section II that for image processing, the optimum mode of operation is to use an ultra-thin nonlinear Fabry-Perot. The use of the ultra-thin geometry ensures that diffraction does not blur the pixels. This requires a nonlinear medium (GaAs, InSb, or glass) only 2 μm thick, surrounded by a dielectric reflecting stack. These devices can be fabricated by sputter deposition, a technique well-suited to the needs of the large-area devices desirable for image processing. With this process, a transparent substrate

can be used, and all layers, both the dielectric reflecting stacks and the ultra-thin nonlinear layer, can be deposited. We show that the largest number of bits can be obtained by using InSb at liquid helium temperatures, using a CO laser at 5 μm. We also show that more convenient operation, although fewer bits, can be obtained using GaAs, or absorbing glass.

In addition to the nonlinear Fabry-Perot, we have studied optical bistability in a hybrid electrical/optical configuration, described in section III. This allows the use of the integrated optics format to produce a one-dimensional array of bistable devices for optical signal processing. These hybrid devices require modulators, detectors and amplifiers, all integrated in an array format onto either a combination $LiNbO_3$ - silicon, or onto GaAs. We will show that, using technology which is available and reported today, over 2500 spots in a bistable linear array are possible, with hybrid electrical/optical modulation speed which may approach nanoseconds.

Research has shown that there is not yet one ideal material for the all-optical bistable device since the materials which require the least amount of power also require liquid helium temperatures. For that reason, we have investigated other materials and geometries for optical bistability. These are described in Section IV, and include preliminary experimental results on optical bistability in saturable absorbing dyes. We believe we have demonstrated optical bistability, but that the nonlinear refractive index has a contribution which is comparable to that of the saturable absorber.

We have also begun experiments to observe optical bistability in InAs, using an HF laser near 3 μm. Our experiments show that the bandgap depends very much on the doping level, and that appropriate match with the HF laser lines requires availability of samples with a range of doping levels and/or temperature variation of the samples from room temperature down to liquid helium temperatures.

3

We investigated theoretically several geometries other than the nonlinear Fabry-Perot for all-optical bistability. This includes the use of distributed feedback to replace the discrete mirrors and the investigation of bistability in degenerate four-wave mixing. In each case, we were able to derive exact solutions to the nonlinear Maxwell's equations and demonstrate that bistability is achievable in each of the proposed geometries.

Finally, we have made extensive studies of the dynamic properties of bistable optical devices, both experimental and and theoretical which are described in section V. This study began with the discovery of "critical slowing down" which increases the predicted response times and required switching energies for bistable devices. Under some conditions, we found that estimates of switching energy could be as much as ten times too low if steady-state values were used. We also found a range of new phenomena which arise when the nonlinear medium response time and cavity roundtrip time are comparable, and result from "overshoot switching". Finally, when the roundtrip time is much faster than the response time of the medium (the case of interest in the ultra-thin nonlinear Fabry-Perot), we found that under some conditions (typically high finesse) the states of the NLFP are not stable, but are self-oscillating. The study of these new dynamic effects have increased our understanding of the behavior of bistable optical devices.

The research program has been under the direction of Professor Garmire. During the early phases, contributions were made by Professor John Marburger. Several Research Scientists at the Center for Laser Studies contributed to a research - most notably Drs. Susan Allen, Jeff Goldstone, and Ping-Tong Ho. Finally, graduate students working on the project have been Herbert Winful (Ph.D., 1981) and Craig Poole (Ph.D. in progress).

Table 1-1 lists the publications which have resulted from this program. Table 1-2 lists the talks which the research team gave on work related to this effort. Table 1-3 describes additional activities coupling our research to other groups.

4

TABLE 1-1

PUBLICATIONS ARISING FROM THE CONTRACT

Papers:

1. "Regenerative Oscillations in the Lossless Nonlinear Fabry-Perot" (J. A Goldstone, E. Garmire) J. Quantum Electr., submitted.

2. "Ultra-Short Pulse Detection with Bistable Optical Devices" (E. Garmire, J. A. Goldstone, J. Hendrix) Applied Optics, submitted.

3. "Transient Phenomena in Bistable Optical Devices" (J. A. Goldstone, P.-T. Ho, E. Garmire) Proceedings of the International Conference on Bistability ed. Bowden and Robl, Plenum Press, 1981.

4. "On the Dynamic Response of Nonlinear Fabry-Perot Interferometers" (J. A. Goldstone, E. Garmire) J. Quantum Electr. QE-17 366 (1981)

5. Signal Processing with a Nonlinear Fabry-Perot" (E. Garmire) Proc. SPIE 269 (1981).

6. "Overshoot Switching, Alternate Switching, and Subharmonic Generation in Bistable Optical Devices" (J. A. Goldstone, P.-T. Ho, E. Garmire) Appl. Phys. Lett. 37, 126 (1980).

7. "Introduction to Bistable Optical Devices for Optical Signal Processing" (E. Garmire) SPIE 218 27 (1980).

8. "Hysteresis and Optical Bistability in Degenerate Four-Wave Mixing" (Winful, Marburger) Applied Physics Letters 36 613 (1980).

9. "Progress in Bistable Optical Devices" (Garmire) Proc. SPIE 176, 12 (1979).

10. "Theory of Bistability in Nonlinear Distributed Feedback Structures" (Winful, Marburger, Garmire) Applied Physics Letters 35, 379 (1979).

11. "Transient Response of Hybrid Bistable Optical Devices" (Garmire, Marburger, Allen, Winful) Appl. Phys. Lett. 34 374 (1979).

12. "Transient Switching Phenomena in Bistable Optical Devices"
    (P.-T. Ho, J. A. Goldstone, E. Garmire) International Quantum
    Electronics Conference, 1980.

13. "Overshoot Switching in Bistable Optical Devices" (J. A. Goldstone,
    E. Garmire, P.-T. Ho) Topical Meeting on Integrated Optics, 1980.
    Transient Response of Bistable Optical Switches" (Garmire,
    Marburger, Allen, Winful) Conf. Laser Eng. and Applic. Washington
    D.C. 1979.

14. "Theory of Optical Bistability in Nonlinear Distributed Feedback
    Structures" (Winful, Marburger, Garmire) Opt. Soc. Am.
    Rochester, 1979.

15. "Calorimetric Measurement of $LiNbO_3$ Waveguide Absorption
    Losses" S. D. Allen, E. Garmire, M. Bass, B. Packer,
    Appl. Phys. Lett. 34 435 (1979).

TABLE 1-2 TALKS ARISING FROM THE CONTRACT

Invited Talks:

"Tomorrow's Optics" (E. Garmire) Society of Women Engineers
National Convention, 1981.

"Signal Processing with a Nonlinear Fabry-Perot" (E. Garmire)
SPIE, Los Angeles 1981".

"Introduction to Optical Bistable Devices" (E. Garmire) Opt.
Soc. of Rochester, New York, 1981.

"Operating Characteristics of the Bistable Nonlinear Fabry-Perot"
(E. Garmire) 1980 Annual Meeting of the Optical Society of America.

"Transient Phenomena in Bistable Optical Devices" (J.A. Goldstone,
P.-T. Ho, and E. Garmire) Second International Conference on
Optical Bistability, 1980.

"Bistable Optical Devices and their Dynamic Response" (E. Garmire)
Sergio Porto Memorial Conference, 1980.

"Optical Bistability" (E. Garmire) Symposium on Spectroscopy,
Quantum Electronics and Astrophysics to celebrate the 65th
Birthday of C. H. Townes, 1980.

"Transient Response of Hybrid BOD's", (J.A. Goldstone, P.-T. Ho,
and E. Garmire) American Vacuum Society, Anaheim, April 1980.

"Optical Bistable Devices" (E. Garmire) Optical Society of
Southern California, 1980.

"Progress in Bistable Optical Devices" (Garmire) SPIE,
Washington 1979.

"Bistable Optical Switches" (Garmire, Allen) Soc. Women
Engineers, San Francisco, 1979).

"Bistable Optical Devices for Integrated and Fiber Optics Applications"
(Garmire, Allen, Marburger) SPIE, Washington, 1978

"Bistable Optical Devices: An Overview" (Marburger, Garmire) Physics
of Fiber Optics, Rhode Island, 1978

Contributed Talks

"Ultrashort Pulse Detection with Nonlinear Fabry-Perots"
(E. Garmire, J. A. Goldstone, J. Hendrix) CLEO Washington,
1981.

"Transient Analysis of the Absorptive and Dispersive Fabry-Perot"
Interferometer" (J.A. Goldstone, E. Garmire) Annual Meeting of the
Optical Society, 1980.

"Regenerative Oscillation in the Nonlinear Fabry-Perot"
(J.A. Goldstone, E. Garmire) Opt. Soc. Am. Annual Meeting,
1981.

"Transient Switching Phenomena in Bistable Optical Devices"
(P.-T. Ho, J.A. Goldstone, E. Garmire) International Quantum
Electronics Conference, 1980.

"Overshoot Switching in Bistable Optical Devices"
(J.A. Goldstone, E. Garmire, P.-T. Ho) Topical Meeting on
Integrated Optics, 1980

"Transient Response of Bistable Optical Switches" (E. Garmire,
J. Marburger, S.D. Allen, H. Winful) Conf. Laser Eng. and
Applic. Wqshington, DC 1979.

"Theory of Optical Bistability in Nonlinear Distributed
Feedback Structures" (H. Winful, J. Marburger, E. Garmire)
Opt. Soc. Am. Rochester, 1979.

TABLE 1-3

ADDITIONAL ACTIVITIES ON BEHALF OF THE CONTRACT RESEARCH

1. Visitors at USC in the field of Optical Bistability
    Peter Smith, Bell Laboratories
    Jack Tomlinson, Bell Laboratories
    Desmond Smith, Herriot Watt University
    Ken Lau, California Institute of Technology
    Hyatt Gibbs, University of Arizona

2. Prof. Garmire was chair of the panel discussion on the
    applicability and the limitations on bistable optical devic
    for the Second International Conference on Optical Bistabil   .
    The discussion was published in the Conference proceedings.

3. Prof. Garmire visited the following institutions and described
    the work at USC based on bistability to interested people.
    Formal Talks:
    Rockwell Science Center
    RADC
    IBM Research Laboratories
    Stanford University
    Informal Discussions:
    Hughes Research Laboratories
    Naval Research Laboratories
    National Security Administration
    The Aerospace Corporation
    General Dynamics
    McDonnell Douglas Corp.
    University of Rochester

B. INTRODUCTION TO BISTABLE DEVICES

The classic geometry for the bistable optical device is the nonlinear Fabry-Perot (NLFP) which is shown in Figure 1-1, along with its transmission and transfer curves. An understanding of the nonlinear transfer curve can be obtained in a simple manner from the figure. Consider the device operating at low intensity levels at the point on the transmission curve designated by the arrow. Because of the nonlinear index, an increase in intensity causes a decrease in effective wavelength and a corresponding increase in transmission. The resulting transfer curve shows optical bistability - that is, two possible stable output states for a given input intensity level. In addition to the bistability, the strong nonlinearity of output with respect to input raises the possibility of interesting optical processing methods.

The image processing function of the thin nonlinear Fabry-Perot is shown schematically in Fig. 1-2. If the Fabry-Perot is biased in the nonlinear regime, the weak inputs are only weakly transmitted, while slightly higher inputs are much more strongly transmitted. This represents image enhancement.

The optical processing techniques available with the nonlinear Fabry-Perot are shown in Fig. 1-3. The input is plotted as a function of position going down and the output is plotted as a function of position going left. This particular representation is especially useful to demonstrate the image processing applications of the nonlinear Fabry-Perot. Differential optical gain (Figure 3a) can be used to improve signal-to-noise. This makes possible optical discrimination, background suppression, and contrast enhancement. Optical limiting (Figure 3b), occurs because the flat output of the nonlinear Fabry-Perot as a function of input makes possible level slicing, with clipper action, and saturated output. A multistable Fabry-Perot can be achieved with higher input powers and leads to a digital output for analog input. The level slicing makes possible an optical AND function, shown in Fig. 1-4. For the two additive input signals shown, the
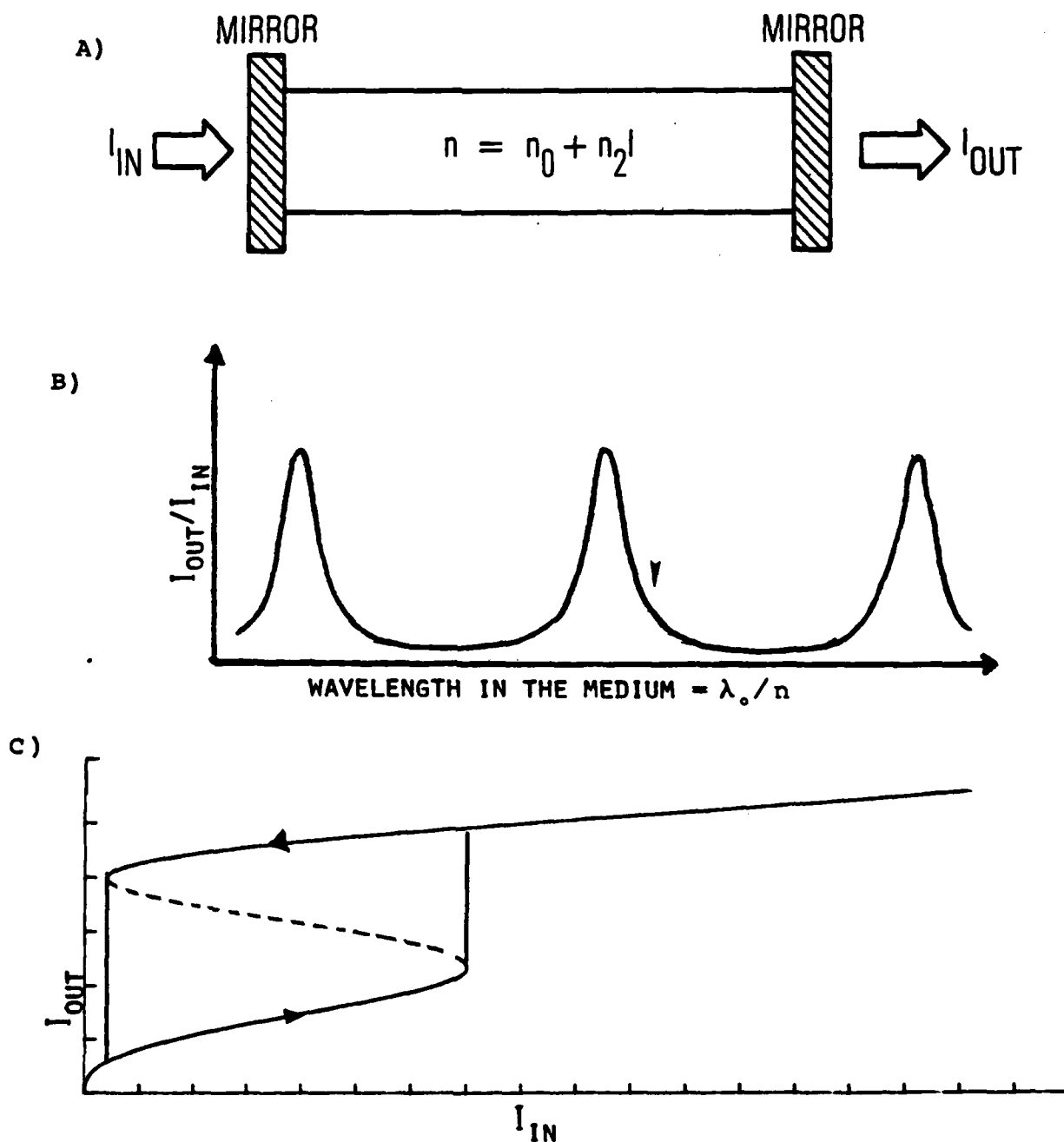
10

A) MIRROR MIRROR

I_{IN} $n = n_0 + n_2 I$ I_{OUT}

B)

I_{OUT}/I_{IN}

WAVELENGTH IN THE MEDIUM = λ_o / n

C)

I_{OUT}

I_{IN}

Figure 1-1. Optical bistable nonlinear Fabry-Perot.
a) Geometry under consideration
b) Transmission as a function of wavelength in the medium (inversely proportional to refractive index)
c) Transfer curve (output vs input) showing bistability

Figure 1-2. Image processing in a thin nonlinear Fabry-Perot.
Density of dots represents relative ir ensity. The nonlinear
image processing in the Fabry-Perot causes an enhancement of
the strong portions and a suppression of the weaker portions of
the image.

ORIGINAL IMAGE
PLANE

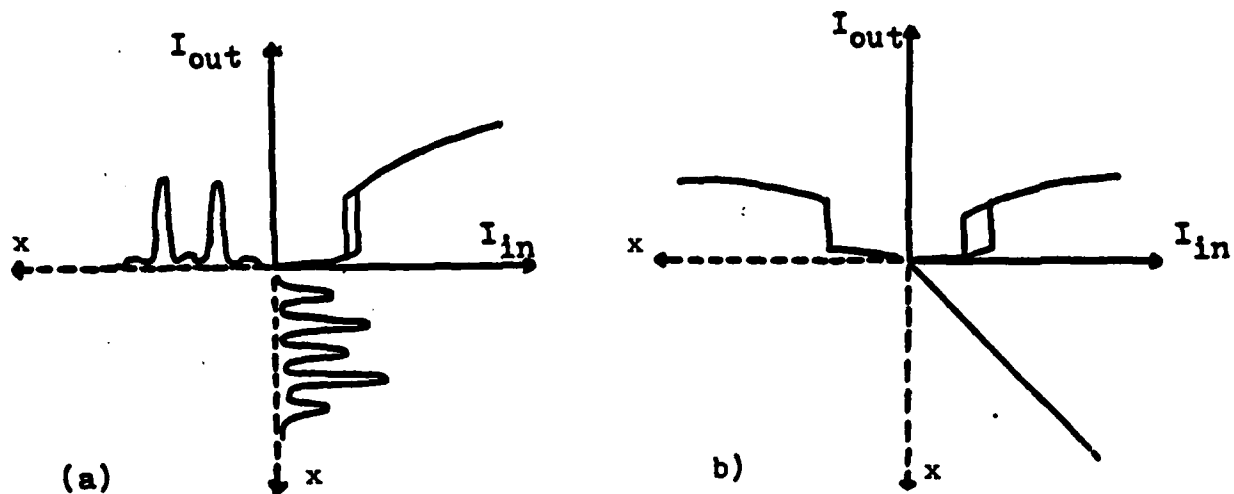NONLINEAR   ENHANCED IMAGE PLANE

FABRY-PEROT

12
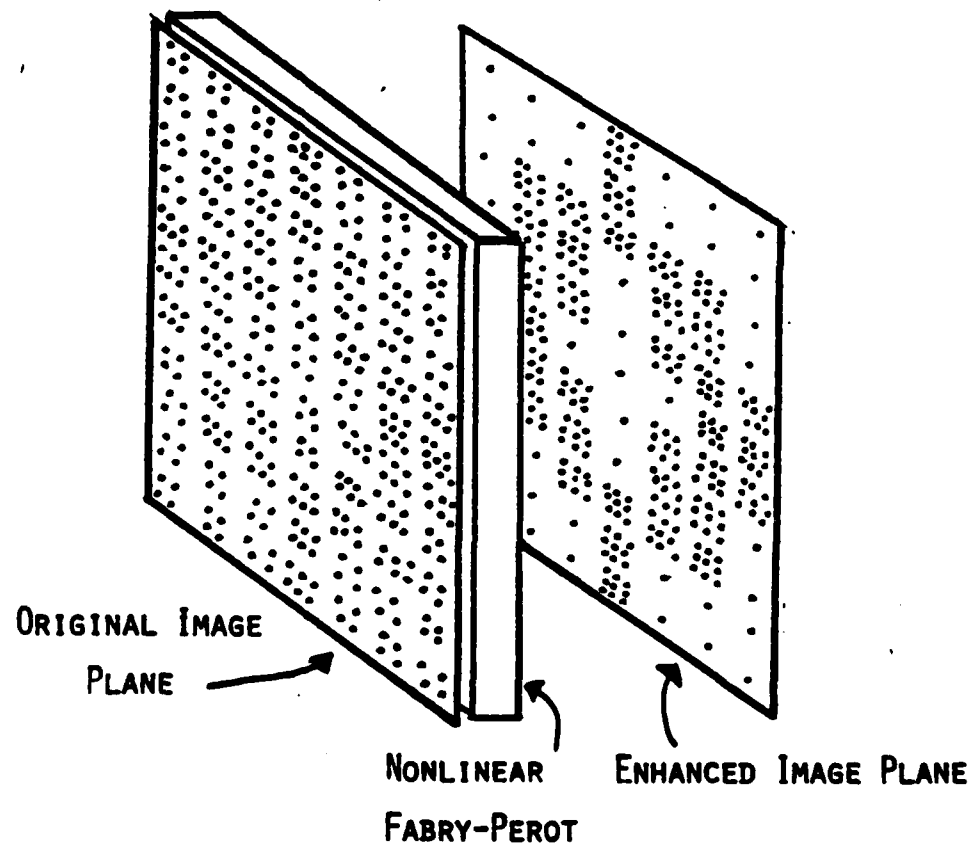
Figure 1-3 Two modes of operation of the nonlinear Fabry-Perot.
In each case the functional dependence of the input is shown,
running down, while the functional dependence of the output is
shown running to the left. The variable can be considered to
be the linear distance across the Fabry-Perot describing image
information. (a) demonstrates differential optical gain, while
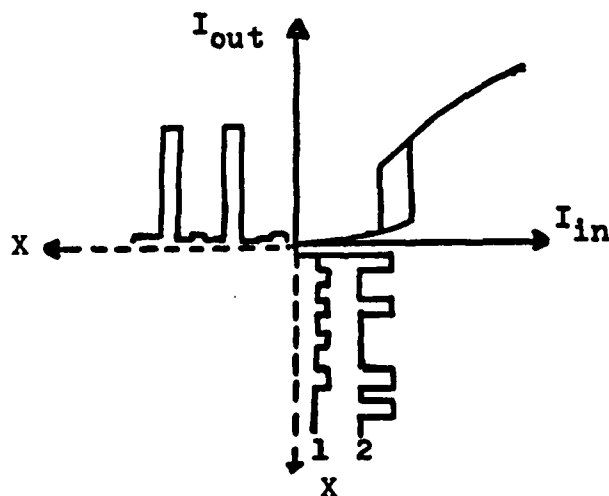(b) demonstrates optical limiting.

Figure 1-4. Optical AND circuit.
a large output results only when
both inputs are present.

output is large only when both signals are present. Thus two images can be compared and only those features which are in both will be transmitted.

The optical memory function which is available because of the hysteresis requires a certain holding optical power. If this is available, the device retains a memory of its previous signal. This is useful for image retention, allowing one image to be compared to another received later in time. Figure 1-5 shows how a multiple-stable-state Fabry-Perot is used to retain one image, and compare it with another occurring later in time. The device retains information as to positions at with both images are bright, as well as positions at which only one image is bright. The multistable Fabry-Perot is obtained by driving the nonlinear Fabry-Perot at higher input intensities than used to achieve bistability.

What is not transmitted through a Fabry-Perot is reflected. The reflected transfer curve can be used to develop a device to obtain one of the functions required for optical computing: The exclusive or. To obtain this function requires an output which is periodic in input intensity, so that two "ones" add to a zero. The reflection from a NLFP is such a periodic function. An exclusive or can be constructed as shown in Figure 1-6.

Figure 1-5. Multistable nonlinear Fabry-Perot used for image comparison and retention of matching information: (a) multistable transfer curve, image input and output remaining after first input is removed. Second image input is also shown, dotted. (b) Multistable transfer curve and input of second image summed with the output remaining after the first image is removed. The output has three possible states: the highest is achieved only in areas where both images were bright; the middle intensity level is obtained where one or the other images are bright, but not both; the third is obtained where neither image was bright. The output is shown after both images are removed. In this optical memory is contained the comparison between the two images.

15
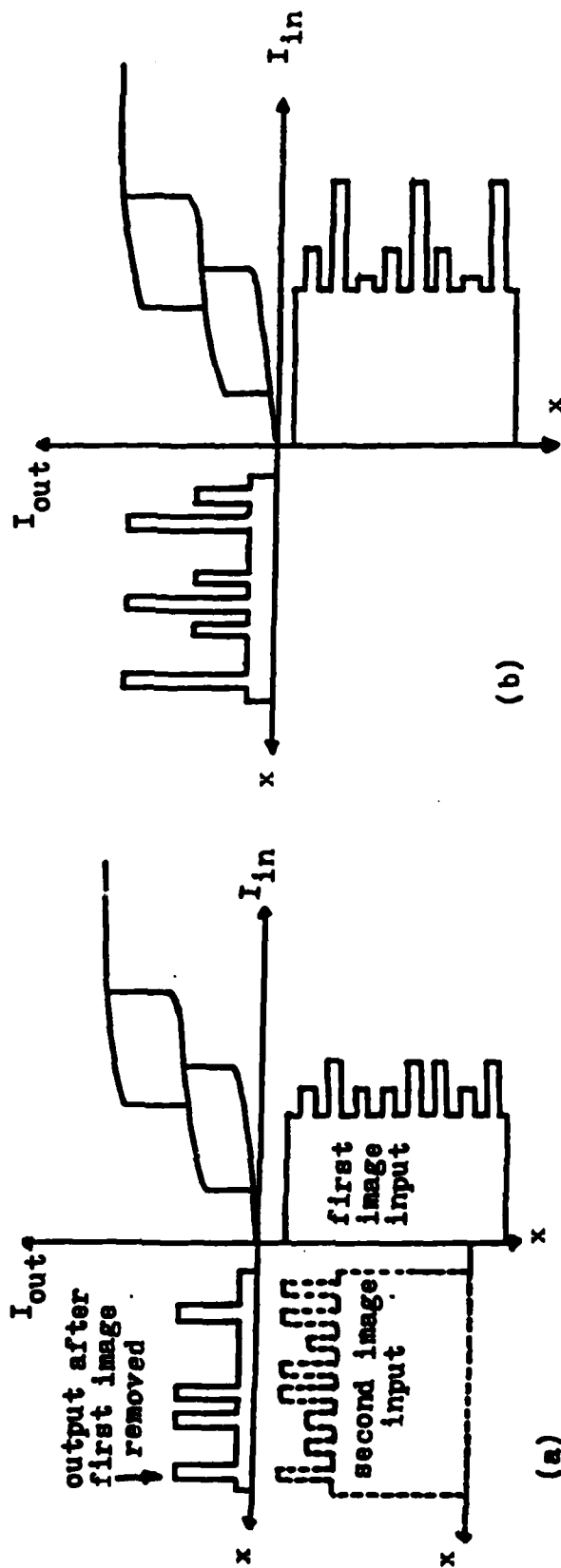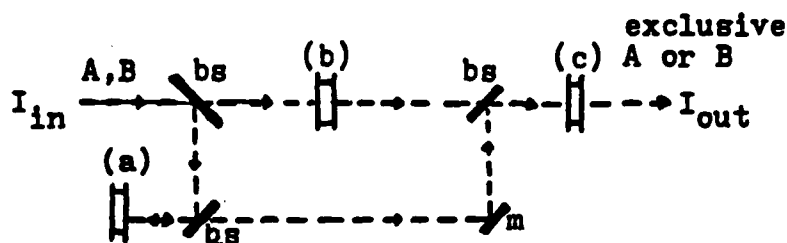
a. Diagram of arrangement of nonlinear
Fabry-Perots (a), (b), (c) which combine to
yield an exclusive OR. bs is beam splitter,
m is mirror. For A,B incident, transmitted
light is the exclusive A or B.
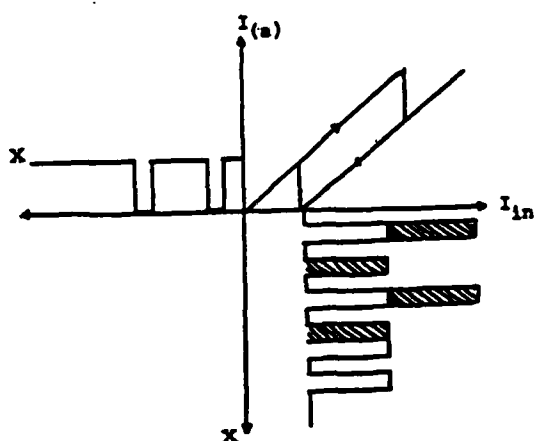
b. Signal reflected from nonlinear
Fabry-Perot (a) as first step in the exclusive
OR
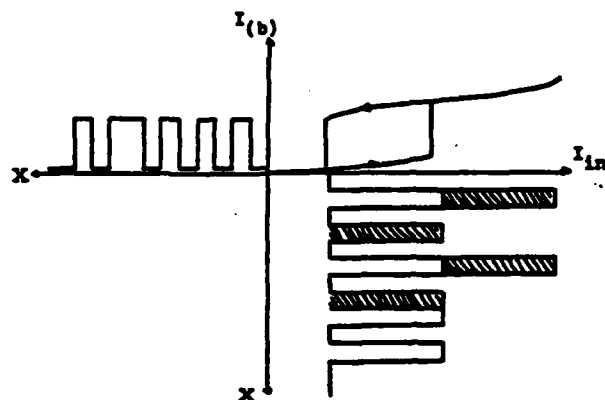
c. Signal transmitted through nonlinear
Fabry-Perot (b) as the second step in the exclu-
sive OR.

Figure 1-6. Exclusive OR output of the combination of nonlinear
Fabry-Perots shown in a. The final signal is obtained by adding
the signals from (a) and (b) in a third nonlinear Fabry-Perot,
shown as (c).

16

II. IMAGE PROCESSING WITH BISTABLE DEVICES

Nonlinear optical devices utilize the optical properties of materials to produce nonlinear optical signal processing. In principle these process can be very fast, since they do not require electronics. For example, the nonlinear refractive index of materials like CS_2 have speeds of psec. It is thi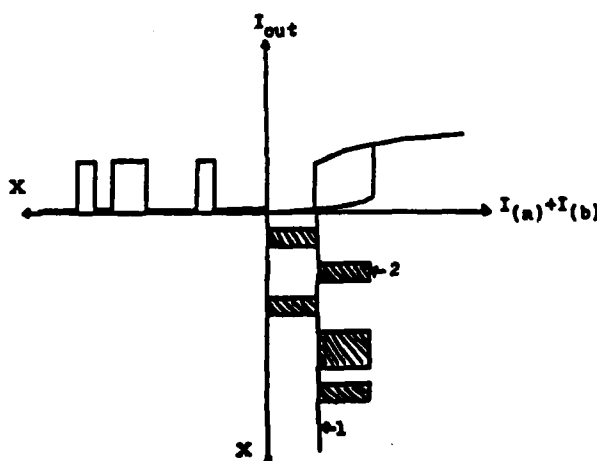s fact which has spurred research in nonlinear optical signal processing devices such as the bistable devices. Indeed, discussion has been made of the possibility of optical computers utilizing this very fast switching time.

Because nonlinear refractive indices tend to be small, nonlinear optical effects tend to require high incident light levels. The limit on the number of resolvable spots which are useful for optical image processing is determined by the intensity levels necessary for switching and the minimum area which can be achieved for each spot. We examine here the conditions to obtain high resolution image processing with bistable optical devices, and find that under the appropriate conditions, as many as 10^6 resolvable spots with speeds as fast as a nanosecond may be achieved.

The Fabry-Perot has been used for optical image processing by Bartholomew and Lee (Applied Optics 19, 201 (1980)), using a spherical resonator to obtain a large number of resolvable spots. We have considered the possibility of image processing in an ultra-thin Fabry-Perot. These devices have an inherent advantage over the spherical cavity considered by Bartholomew and Lee in not requiring a careful frequency match between laser frequency and the cavity resonance frequency, reducing the cavity stability requirements. An ultra-thin Fabry-Perot is considered to contain a material with a nonlinear refractive index, and some residual linear absorption. The research to date has predominantly involved optical processing of single elements. There are, however, several demonstrated results on bistability in ultra-thin Nonlinear Fabry-Perots (NLFP) which would be useful for image processing. The experimental results are summarized in Table 2-1

17

Table 2-1

Experimental Results on Single Pixel Signal Processing Using Bistability in Thin Nonlinear Fabry-Perots.

Medium	Thickness μm	Wavelength μm	Intensity $MW/\mu m^{2-}$	Power/ Pixel	Speed
Absorbing glass (refs. 1,2,3)	57	0.63	.08	20 mW	100 μsec
GaAs (refs. 1,2,4)	4	0.82	1	4.2 mW	40 nsec
InSb (ref. 5)	580	5	.01	50 mW	~nsec

References

1. H.M. Gibbs, et.al., Appl. Phys. Lett. 34, 511 (1979).
2. H.M. Gibbs, Et.al., Fourth International Conference on Laser Spectroscopy, West Germany, 1979.
3. McCall, J. Opt. Soc. Am. October, 1978.
4. H.M. Gibbs, et.al., Appl. Phys. Lett. 35, 451 (1979).
5. D. Smith, D.A.B. Miller, Appl. Phys. Lett. 35, 658 (1979).

The limitation on the resolution of the thin Fabry-Perot is diffraction which occurs in the several passes that the light makes through the interferometer. The minimum spot size which can maintain itself at its diameter without diffracting for a distance L_{eff} is given by

$$D = (2 \lambda_o L_{eff}/n)^{\frac{1}{2}} \tag{1}$$

where L_{eff} is the effective path length of the beam through the Fabry-Perot, and is given by $L_{eff} = FL/n$, where F is the finesse.

The number of resolvable spots which may be processed in the image is limited by the available power, since every element must be subject to sufficient intensity to operate in the non-linear regime. D.A.B. Miller (IEEE J. Quantum Electr. QE-17 306 (1981)) has made a theoretical study of the optimization of a NLFP, and found that the critical intensity is given by

$$I_c = \frac{1}{\beta} \frac{1}{\mu_o} \frac{1}{P} \tag{2}$$

where $\beta = \frac{3n_2}{\lambda\alpha}$, proportional to the ratio between the nonlinear index and the linear absorption. P is a parameter which depends on the NLFP reflectivities and can be made close to two and μ_o is a figure of merit which typically lies between 1 and 10, depending on cavity geometry. The only dependence on cavity length is found in μ_o, which is close to inversely proportional to cavity length, for a given nonlinear index and absorption coefficient. This means that the shorter the cavity, the better. The shorter cavity has additional advantages of higher spatial resolution, and less stringent tolerances on the bandwidth of the incident light.

Table 2-1 listed the experimental results to date on thin NLFP's. The power per pixel was calculated by including the finite spot size as expressed in Eq. (1), for each device. It can be seen that in several cases, since the length of the Fabry-Perot was relatively large, the power per pixel was rather high - a consequence primarily of diffraction.

The NLFP geometry is optimized by using the thinnest possible cavity lengths, not only to avoid degradation of spatial resolution due to diffraction, but also to obtain lower critical intensities, as expressed in Eq. (2). Since μ_o is inversely proportional to cavity length, within the range of interest, then the critical intensity is directly proportional to cavity length. This means that decreasing the thickness a factor of ten decreases the critical <u>intensity</u> a factor of ten, the critical <u>power</u> per pixel decreases a factor of one hundred. Thus, the optimum NLFP requires using as short a cavity length as possible. There are, of course, limits to this optimization, since decreasing the cavity length to zero is unphysical. Exact determination of the limits of applicability requires applying the theory of Miller more carefully.

We show in Table 2-2 predicted behavior of ultra-thin NLFP's. For InAs we include the estimated power per pixel based on the above simple arguments, and the estimated power per pixel determined by Miller from a more complete optimization of NLFP parameters in InAs. The fact that he has obtained an additional factor of 25 by more careful optimization indicates that further optimization beyond the values listed in Table 2-2 should be possible with the other devices as well.

Table 2-2

Predicted Theoretical Results for Ultra-Thin Nonlinear

Fabry-Perots For Use With Image Processing

Medium	Thickness μm	Intensity $\mu W/\mu m^2$	Power/ pixel μW	Speed	Energy/ Pixel
absorbing glass	2	2.3	25	100 μsec	2.5 nJ
+ heat sink	2	23	250	10 μsec	2.5 nJ
GaAs	2	500	1050	40 nsec	42 pJ
InSb	6	0.1	1	1 nsec	1 fJ
+ further optimization		.004	.04	1 nsec	.04 fJ

A careful look at Table 2-2 allows us to make some very inter-esting predictions about image processing with a NLFP. Consider first the absorbing glass NLFP. This device relies on the change in refractive index due to localized heating of glass occurring because of optical absorption. The results to date were for a device 57 μm thick. This is as thin as a bulk piece of glass can be polished. Signal processing using an ultra-thin glass NLFP will require obtaining thin glass films ~ 2 μm thick with properties comparable to the thicker films. We suggest that sputter deposi-tion of a thin glass film will be the process by which to obtain the thin film. Good quality glass films have been sputtered, and in fact made into optical waveguides. For the NLFP, dopants will be added during sputtering to ensure the proper amount of absorption in the glass.

In the absorbing glass NLFP, the nonlinearity is effectively dependent on the absorption since it is caused by thermal heating. This means that optimization requires looking at the thermal heating properties of the device. Both the sensitivity and speed of the device are related to the thermal conductivity. We present here a simple modeling of the thermal bistable device.

In order to determine the temperature rise, and therefore the change in refractive index due to the absorption of a given fraction of the incident light intensity, we require that the heat flow into the sample equals the heat flow out of the sample. The relationship equating these two is:

$$\alpha \, L \, A \, I \, \tau = A \, L \, \rho \, C \, \Delta T$$

where α is the absorption coefficient, L the length of the Fabry-Perot, I the incident intensity, A its area, and τ the thermal time constant of the particular geometry under consideration, ρ is the density and C the specific heat. The temperature rise ΔT causes the change in refractive index through $\Delta n = (dn/dT)\Delta T$, so that the refractive index rise can be written as

$$\Delta n = \frac{(dn/dT)\tau\alpha}{\rho C} I \equiv n_2 I \quad . \tag{3}$$

Thus the nonlinear index, n_2, is proportional to the absorption coefficient but does not explicitly depend on the length of the sample. This means that the modeling by Miller which was appropriate for the nonlinear Fabry-Perot is also valid for the thermal nonlinearity.

The nonlinear index does, however, depend on the response time of the sample. The response time may be decreased by heat sinking the sample, but it will be at a cost of a decrease in the nonlinear index.

A related problem is the requirement to reduce the heat flow in the plane of the Fabry-Perot which would decrease the spatial resolution of the image processor. As long as a thin Fabry-Perot is considered, on a heat-sink substrate with conductivity substantially larger than that of the glass, there should be no problem with loss of resolution. As an example, we consider a conductivity sufficient to improve the response time an order of magnitude, causing a related decrease in nonlinear refractive index by an order of magnitude. The results are shown in Table 2-2.

The ultra-thin absorbing glass filter, on an appropriate heat sink (such as sapphire) requires 250 μW per pixel, so that a 2.5W laser will be able to process 10^4 spots, with a time constant of 10 μsec. This is considerably better than any spatial light modulator available today. Furthermore, an order of magnitude more pixels can be processed with a time constant of 100 μsec by eliminating the heat sink. By com-

parison, the GaAs NLFP requires forty times more power, so can process forty times fewer spots, but is at a speed 1000 times faster.

The NLFP with the lowest required power is InSb, in which a power per pixel of 1 μwatt leads to the possibility of processing 10^6 pixels in 1 nsec with a 1 watt laser. The only drawback of this material is the fact that it operates at 5 μm, with a CO laser, at low temperatures, which is not very convenient for systems applications.

The reference by D.A.B. Miller shows that a complete optimization of all the parameters available in designing a nonlinear Fabry-Perot makes a predicted switching power for the InAs device 6 μm long of 4 nanowatts rather than the 100 nWatts we predicted from simple arguments above. At this power level, the predicted power per pixel is 40 nWatts, so that a 4 watt laser would produce 10^8 resolvable spots in 1 nsec. Such a device has astounding possibilities for signal processing.

The ultra-thin Fabry-Perot has several other advantages for image processing. Both the frequency and angular acceptance bandwidths are relatively large. Consider, for example, the wavelength acceptance bandwidth of a Fabry-Perot 2 μm thick. The width of the resonance is given by

$$\Delta\nu = 1/2nLF$$

where L is the length, F is the finesse, and n is the refractive index. We find $\Delta\nu/\nu$ = .025, or $\Delta\lambda$ = 150Å. This wide bandwidth means that no special precautions are required on the light source which is used. In principle, an incoherent light source could be used if it were filtered to 150 Å. The second consideration is the acceptance angle of the Fabry-Perot. This can be calculated by imagining the Fabry-Perot is on resonance and calculating the angle at which the Fabry-Perot goes out of resonance.
We obtain

$$1 - \cos\theta = n\lambda/2LF \cdot$$

When the Fabry-Perot is 2 μm thick, with a finesse of ten,

this is 14°. The optical system which most favorably will couple to this NLFP is f4, a perfectly reasonable requirement for an optical system.

The NLFP can be used in image processing in two ways. First, in a cw fashion, in which the image is impressed on the incident laser beam through such means as a photographic plate or other imaging device. The NLFP can also be used in the scanning mode, with the image impressed by intensity modulation on a scan beam. In this mode of operation, the NLFP essentially processes pulses of light, and the processed image will be recorded in suitable fashion, for example, on a detector array or photographic plate. In this case, it is the energy for switching a pixel in a pulse which is important. This information is shown in the last column in Table 2-2. It can be seen that GaAs has a decided advantage over the absorbing glass in this usage, and that InSb is again an optimum material. Assuming that a four watt laser is used, 10^{11} bits can be processed per second using a GaAs NLFP, while only 2×10^{9} can be processed in the absorbing glass NLFP. By contrast, at least 10^{15} bits per second can be processed in the InSb NLFP. The very large size of these numbers motivates further research into the NLFP and optical bistability.

III. HYBRID ELECTRICAL OPTICAL BISTABLE OPTICAL DEVICES

In Chapter II we have discussed the nonlinear Fabry-Perot, as a useful bistable device for optical image processing. In this program, we have also made extensive studies of hybrid electrical-optical geometries for bistable optical devices (BOD). While these hybrid devices will not be able to have speeds faster than that of electronics, they may be used in a parallel processing fashion thereby providing overall bit rates greater than nanoseconds. It is interesting to note that none of the nonlinear Fabry-Perots discussed in the last section has speeds to date which are larger than nanoseconds. Thus a nanosecond hybrid bistable device may provide a viable alternative to the NLFP for many applications.

The generic concept of a hybrid bistable optical device is shown in Fig. 3-1. This device uses a modulator, detects its output, amplifies it, and feeds it back as a voltage across the modulator with an optional bias voltage applied. The instantaneous output of the modulator is

$$I_{out} = I_{in} \, T(V) , \tag{3-1}$$

where I_{in} is the input light intensity and T is the modulator transmission function, which depends on the control voltage V. Assuming the detector is linear with detectivity factor δ, and fast, the current $i = \delta I_{out}$. Again, assuming the amplifier is linear and fast, with amplification factor γ, the voltage applied to the modulator is given by $V = \delta\gamma I_{out}$. When the detector and amplifier are not negligibly fast, transient effects are observed, as described in Section V. If the detector and amplifier are not linear, Eq. (3-1) applies with appropriate functional relationships to describe the voltage across the modulator in terms of I_{out}.

Bistability comes from relating the input and output through the transmission:

$$I_{in} = I_{out}/T(\delta\gamma I_{out} + V_B) . \tag{3-2}$$
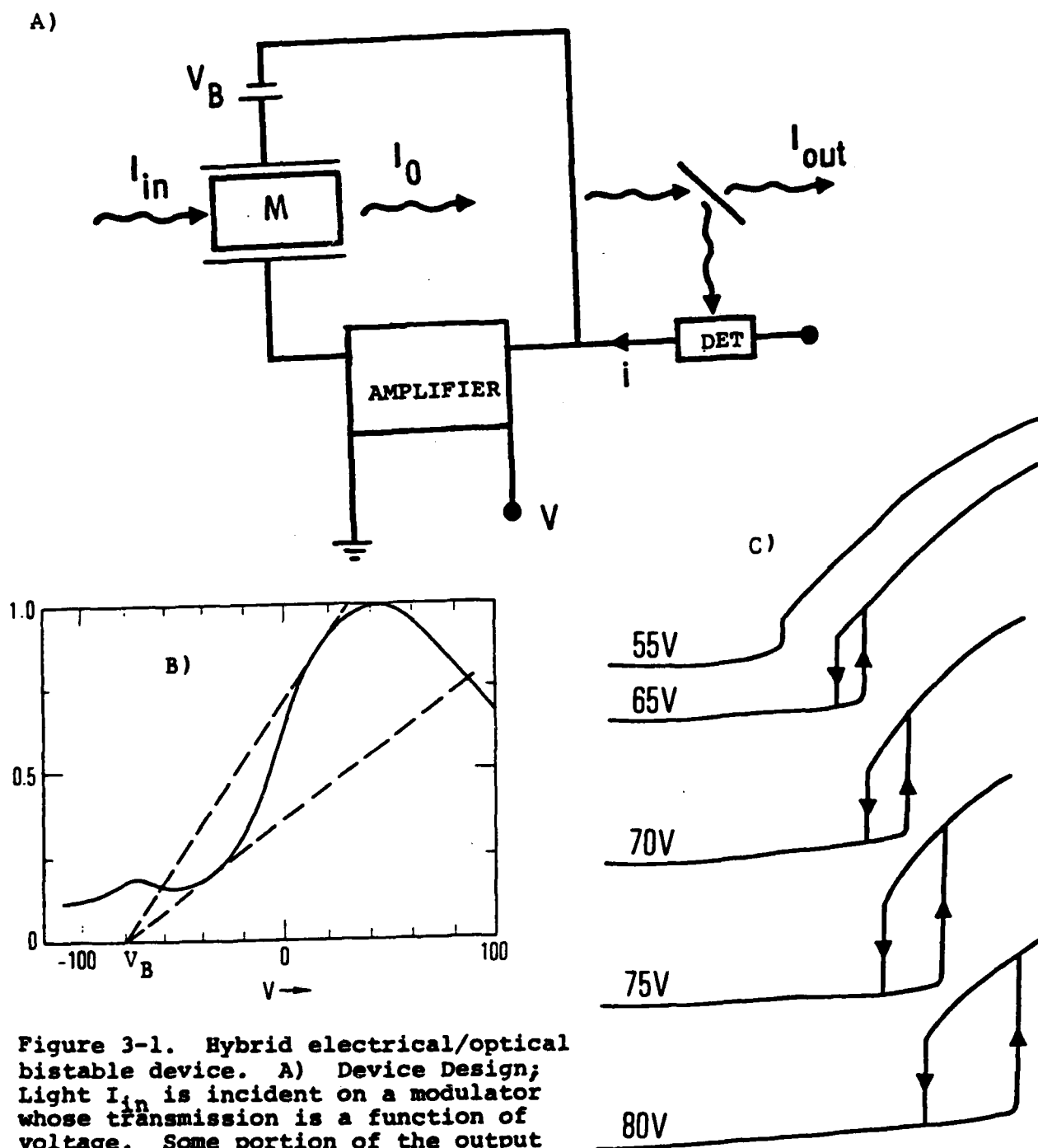
A)

B)

C)

55V

65V

70V

75V

80V

Figure 3-1. Hybrid electrical/optical
bistable device. A) Device Design;
Light I_{in} is incident on a modulator
whose transmission is a function of
voltage. Some portion of the output
light is detected, amplified and fed
back as a voltage on the modulator.
B) Transmission of the experimental modulator as a function of volt-
age. Regions of bistability lie between two lines (of slope $\sim 1/I_{in}$)
originating in V_B which intersect the transmission curve in more
than one point. Notice that a monotonic transmission function may
still cause bistability. C) Experimental transfer curves (Output
vs. Input) for several bias voltages.

Since it is possible for the right hand side of Eq. (3-2) to
have the same value for several values of I_{out}, it is possible
to have the same value of I_{in} lead to several values of I_{out}.
This causes bistability or multi-stability.

We demonstrated experimentally that bistability may occur
even if the transmission is a single-valued function of the
voltage as shown in Fig. 3-1. This figure also shows the
graphical solution of the bistable device, determined by the
intersection of a straight line of slope proportional to
I_{in}^{-1} and the transmission function. This solution comes
from equating both sides of the following equation:

$$\gamma \delta I_{out} \left(\frac{1}{I_{in}} \right) = T \ (\gamma \delta I_{out} + V_B) \quad . \qquad (3-3)$$

The existence of bistability in a simple hybrid configur-
ation using a wide variety of transmission functions suggests
the versatility of this approach for optical signal processing.

There are a number of modulators and/or switches in
which hybrid bistability has been demonstrated. The
search for the optimal hybrid bistable device for optical
signal processing is a search for a high-speed low-voltage
modulator and development of the appropriate high-speed
amplifier.

In this section we make a brief review of possible modula-
tors for use with the hybrid bistable device and suggest a
device which we believe is the most appropriate for use in
hybrid BOD arrays for parallel processing.

The simplest concept for an electro-optic modulator is
phase modulation. Kaminow et.al. (Appl. Phys. Lett. 37 555,
(1975)) have demonstrated phase modulation with half-wave
voltages of less than one volt for y-cut, x-propagating $LiNbO_3$
waveguides using electrodes 3 cm long and separated by 9 μm.
To be useful for bistability, the phase modulator must be con-
verted into intensity modulation, however.

Interference of phase-modulated light with background unmodulated light to achieve hybrid bistability was demonstrated by Garmire et.al. (Opt. Lett. 3 69 (1978)) with electrode spacing of 10 μm and electrode length of only 2 mm (half-wave voltage of 80V).

Phase modulation is turned into polarization modulation by placing the device between crossed polarizers as demonstrated in the first hybrid BOD without optical feedback (Garmire, et.al., Appl. Phys. Lett 32 320 (1978)). High speed results of polarization modulation in an integrated optics format were reported· by Izutsu et.al., (IEEE J. Quantum Electr. QE-14 394 (1978)) who observed 64% modulation at 2 GHz using electrodes 35 μm wide and 9 mm long. This device is eminently suitable for a hybrid BOD.

Phase modulation can also be turned into intensity modulation by inserting in a Fabry-Perot resonator. This was used by Smith et.al., to demonstrate the first hybrid BOD (Appl. Phys. Lett. 30 281 (1977)). An integrated optics version was fabricated by cleaving x-cut $LiNbO_3$ in the appropriate direction (32.75° between z and the cleavage plane). They obtained a half-wave voltage of 1.2V for a 12 mm resonator, using the extra-ordinary ray, and a half-wave voltage of 5.5V for a 8.7 mm resonator using the ordinary ray (Smith et.al., Appl. Phys. Lett. 34 63 (1979)).

The use of a resonator has the advantage that it decreases the voltage which must be applied to the modulator to cause bistability. If the resonator has a finesse F, the required voltage is reduced from the half-wave voltage, $V_{\frac{1}{2}}$, to $V_{\frac{1}{2}}/F$. However, the use of a resonator of reasonable length (required to reduce the half-wave voltage) also increases the alignment problems and requires a narrow-band input source. For this reason, the electro-optic Fabry-Perot is not the most convenient hybrid BOD.

One of the most versatile integrated optics modulators is the directional coupler. This has been used in a hybrid

BOD (Cross, Schmidt, Thornton, Smith IEEE J. Quantum Electr. QE-14 577 (1978)). The reported half-wave voltage was 2 V, with a separation between electrodes of 3 μm and length of 2 cm. The detector was an avalanche photodiode with 30A/Watt, and hysteresis was seen with 10 nanowatts of optical power. However, in order to switch with this low incident signal, it was necessary to integrate the detector charge in order to build up sufficient voltage. Thus the switching time was the order of fractions of milliseconds.

Faster hybrid directional coupler switches require amplifiers. One such device was reported by Tarucha, Minakata and Noda (IEEE, JQE 17 321 (1981)) with switching up to 300 MHz using a Ge avalanche photodiode and wide-band amplifier. This device used z-cut, x-propagation in LiNbO$_3$, with a 15 mm interaction length and 4.7 μm separation. A wide variety of directional coupler modulators are currently available to be used in hybrid configuration.

Another modulator type is the interferometric modulator, using branching waveguides such as reported recently by Leonberger (Opt. Lett. 5 312 (1980)), who observed modulation up to 1.4 GHz with 3 mm electrodes separated by 4 μm and a half-wave voltage of 4.5V. Optical bistability has been investigated in a hybrid BOD using an integrated two-arm interferometer (Schnapper, Papuchon, Puech, Opt. Comm. 29 364 (1979)). Using an electrode spacing of width 4 μm and electrode lengths of 5 mm, they observed a half-wave voltage about 10V. They used a photomultiplier to create the voltage sufficient to drive the modulator, and had a response time limited by the RC of the photomultipler circuit. A similar interferometric modulator was used with a phototransistor and amplifier of bandwidth 25 kHz to obtain a hybrid BOD with 6 μsec time constant. (Ito, Ogawa and Inaba, Electr. Lett. 16 543 (1980)). Both the directional coupler and interferometric modulator represent excellent candidates for fast, single-element hybrid BOD's.

A particularly promising type of electro-optic modulator for use as a BOD is the waveguide-cutoff modulator, reported

in a hybrid configuration (W. Sohler, Appl. Phys. Lett. 36 351 (1980)). This device is a Ti-diffused channel waveguide 2 μm wide and only 3 mm long. The application of a voltage is chosen to reduce the refractive index and destroy guiding, causing intensity modulation. The half-wave voltage was 25 V, comparable to a phase modulator of the same length. An amplifier was used and a biasing resistor which caused the time constant to be the order of milliseconds. The usual disadvantage of a waveguide cutoff modulator for modulation applications is that its nulls are shallow, and some light is transmitted even in the "off" state. For optical bistability, however, this is not a drawback, since a non-zero null is required to drive the transfer curve. Thus, the waveguide cutoff modulator may be very useful for hybrid optical bistability.

The electro-optic effect is also used in some other geometries for optical modulation. This may be some form of total internal reflection or some electro-optic grating. Bistability has been seen at the total internal reflection interface between electro-optic KDP and a liquid whose index was close to that of the KDP (critical angle 1°). The device had a half-wave voltage of 1200 V, so is not practical in its reported form (Smith, Tomlinson, Maloney, Kaplan, Opt. Lett. 7 57 (1982)). However, integrated optics versions of the total internal reflection modulator have been reported which could be applicable.

There are several hybrid BOD's which have been demonstrated with modulators which are inherently slow, but have useful features. This includes driving a thin Fabry-Perot with a piezo-electric (McCall, Appl. Phys. Lett. 32 384 (1978)), or an electro-strictive (Gomi et.al., J. Appl. Phys. 20 L375 (1981)) transducer. Typically these devices require drive voltages of hundreds of volts and have response times of milliseconds. A magneto-optic bistable device has also been reported by Umegaki et.al., (Appl. Phys. Lett. 38 752 (1981)).

This device has the advantage of operating with current, rather than with voltage, but the switching time of the reported device was still 0.5 msec because of the inductance in the electromagnetic coil. Better design could speed this up.

Finally, an acousto-optic bistable device has been reported by Albert et.al.(Can. J. Phys. 59 1251 (1981)), operating with a photo-diode + lock-in amplifier + voltage-controlled oscillator + broad-band amplifier. This device has the potential of MHz operation, but the reported BOD demonstrated an unexplained slow temporal drift.

The hybrid BOD will be most useful for optical signal processing if an array of devices can be built. In this way, advantage can be taken of parallel processing (if only in one dimension). The modulators discussed above must be investigated in light of the requirements for a high-density array. In this regard, clearly single-channel modulators will have the advantage. The two most promising are the polarization modulator and the waveguide cutoff-modulator.

An array modulator of the sort which would be useful for a hybrid array BOD has been reported by Xerox Company (Flores, et.al., Integ. Opt. Conf. January, 1982). The device reported had several characteristics which make it useful. First, the driving electronics was fabricated in silicon, using VLSI techniques, which was pressed against the $LiNbO_3$ crystal in close proximity. The fringing fields were the source of electro-optic modulation in the $LiNbO_3$. The device reported had 5376 active elements, formed with parallel metal electrodes. The Xerox array modulator does not make use of integrated optics, but uses a single total internal reflection at grazing incidence to achieve a long interaction length. Some aspects of this design will be useful for a hybrid BOD.

The most practical hybrid BOD array would use a waveguide cutoff modulator with electrodes, detector and amplifier all in a silicon VLSI chip which is proximity-coupled to a $LiNbO_3$ sample. With voltage applied, fringing

fields would create a waveguide, guiding light to the other end of the sample and to the detector array. When no voltage is applied, light would not reach the detector array. Appropriate amplification between the detector and modulator electrodes would be built into the silicon chip using VLSI techniques. Figure 3-2 shows a schematic of such a hybrid BOD array.

Obviously proximity coupling can also be used on other waveguide modulators, such as the polarization modulator. The polarization modulator can be designed to operate at lower voltages than the waveguide cutoff modulator (by fabricating longer devices). However, there is an additional alignment requirements between the modulator electrodes and the channel waveguides.

Another device for a hybrid bistable optical device would be a monolithic construction in GaAs. The modulation, detection and amplifier can all be constructed in GaAs. These techniques have been demonstrated in discrete devices (E. Garmire, Integrated Optics, Ed. Tamir, Springer-Verlag (1975)) and remain to be integrated monolithically.

Two-dimensional hybrid BOD's have been reported using liquid crystal displays, (Sengupta, Gerlach, Collins Opt. Lett. 3 199 (1978), and Athale and Lee, Appl. Opt. 20 1424 (1981)). These devices have the advantage of processing in 2-D, but the slow speed and limited resolution of liquid crystal light valves. The emphasis of our study of hybrid devices has been on developing a high-speed linear array processor.
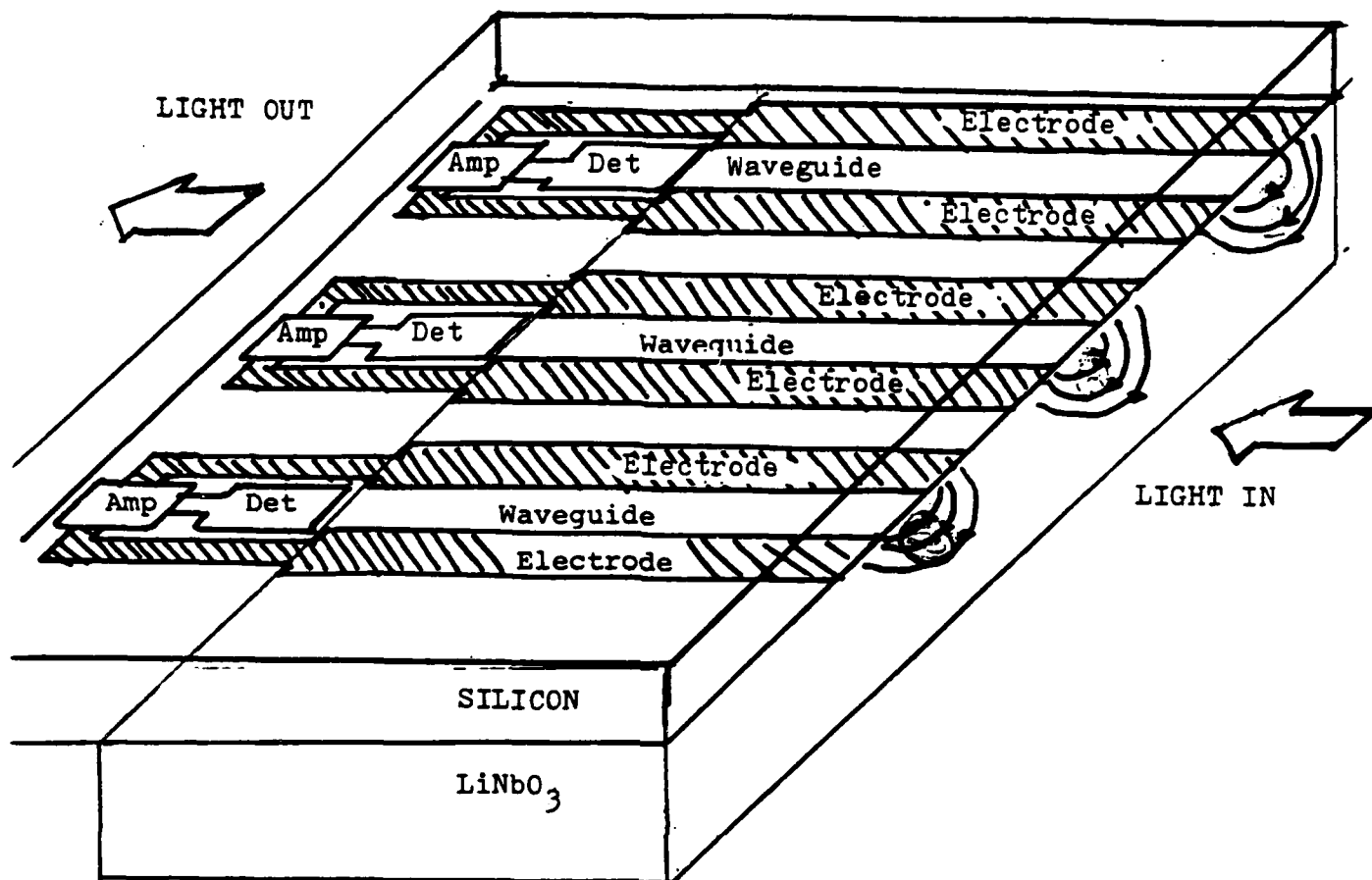
Figure 3-2. Hybrid electrical/optical bistable
array. Electronics structure is in silicon, comprised
of electrodes, detector and amplifier. Optical waveguide
modulator is in $LiNbO_3$. Two substrates are placed face-
to-face, with a press fit. $LiNbO_3$ substrate ends before
the detector, and some portion of the diffracting light
is detected, amplified and fed back. The remaining portion
of the light is imaged with a lens (not shown).

IV. BISTABILITY IN NEW MATERIALS

A. Saturable Absorber Dyes

As part of this program, we have investigated new materials that would be useful for optical bistability. One such material we investigated was saturable absorbing dyes. The desire was to study optical nonlinearities in a material whose composition can be easily varied and that ultimately can be used in an ultra-thin Fabry-Perot. However, the first experiments pursued were in a relatively conventional Fabry-Perot 1 mm thick. The result of this investigation were results which are consistent with bistability. However, in the saturable absorber dyes, there are a number of effects which may take place, and further experimentation on thinner NLFP's is required to prove, without question, that bistability is occurring. In this final report we briefly describe our experimental results on bistability in saturable absorbing dyes.

IV.A-1 Experimental Arrangement

The construction of the Fabry-Perot interferometer and our experimental setup are shown in Fig. 4-1 and Fig. 4-2, respectively. The Fabry-Perot cavity was formed by two plane mirrors with $R_1 = 0.9$ and $R_2 = .95$ separated by three small ball bearings with 0.08 cm diameter. The mirrors were aligned parallel with three screws. Fabry-Perot tuning is achieved by regulating the incidence angle of input laser beam. Input and output pulses of the Fabry-Perot were detected by two photo diodes and photographed simultaneously on a Textronix 7844 dual-beam oscilloscope. We used a single-mode Q-switched Nd:YAG laser with the pulse-width 20 nsec and output of 300 mj. The laser had a Gaussian-beam profile with a maximum peak power of about 15 MW. We used a new dye, bis(4-dimethylaminodithiobenzil) nickel (or BDN) in a dichlorethane solvent as the nonlinear absorber. BDN has a relaxation time which varies markedly with solvent and concentration. With BDN in dichlorethane of concentration 10^{17} cm^{-3}, the relaxation time is about 0.6 ns. Because of the small attenuation loss due to scattering and absorption in dichlorethane solvent the effective mean mirror reflectivity in

Figure 4-1. Construction
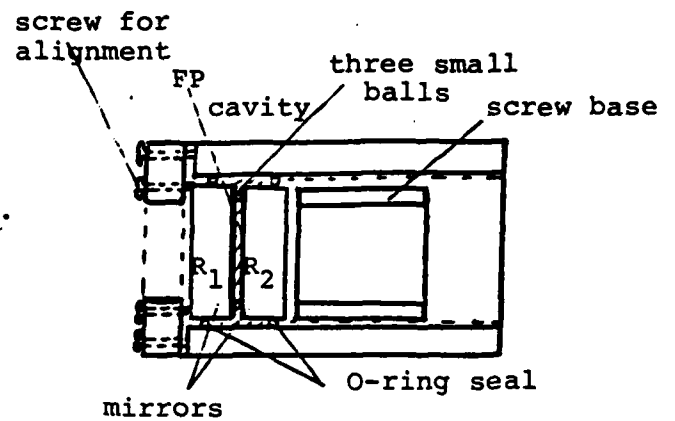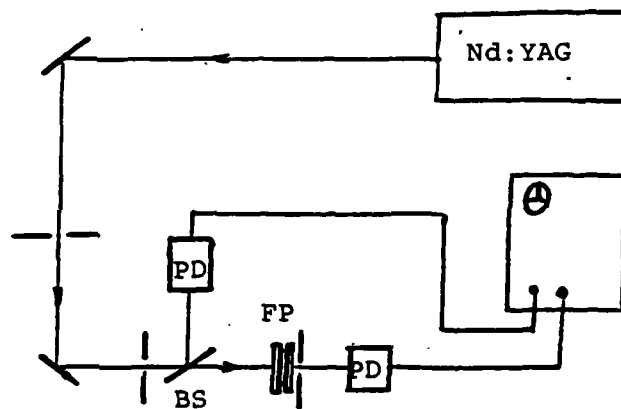of Fabry-Perot Interferometer.

Figure 4-2.
Schematic diagram
of the experimental
setup

BS: Beamsplitter
PD: Photodiode
FP: Fabry-Perot cavity

35

dichlorethane at Nd:YAG laser frequency was about 0.78. The experimentally determined finesse of Fabry-Perot interferometer was 13.

IV.A-2 Absorption Characteristics of BDN

The absorption characeristic of BDN dichlorethane was measured for six concentrations N = (0.5, 1, 1.9, 2.6, 3, 5.1) $\times 10^{17}$ cm^{-3} with the Nd:YAG laser. Figure 4-3 gives the plot of BDN dichlorethane absorption coefficient $\alpha(I)$ vs. input intensity I, where solid curves are theoretical curves calculated from a simple two-level model and the different symbols mean exprimentally measured values for different BDN concentrations. Figure 4-3 shows that the experimental curves can be fitted to the curves derived from theory with $I_s = 9 \times 10^5$ W/cm^2, $\sigma_1 = 1.7 \times 10^{-16}$ cm^2, $\sigma_2 = 2.4 \times 10^{-17}$ cm^2 where $\alpha_1 = \sigma_1 N$ and $\alpha_2 = \sigma_2 N$. The measurement of BDN absorption coefficient provides us with the following data: BDN absorption cross section $\sigma = \sigma_1 + \sigma_2 = 1.94 \times 10^{-16}$ cm^2, the saturable absorption intensity $I_2 = 9 \times 10^5$ W/cm^2, the relaxation time $t = 0.57$ nsec using $t = h\nu/2\sigma I_s$. The latter is very close to the value given by Greenhow and Sereet with the two-photon fluorescence method. The measurments give BDN unsaturable loss of about 12% using α_1. Figure 4-3 also shows that for lower concentrations, or $I \gg I_s$, the experimental results are in good agreement with the theoretical model. However, for higher concentrations and $I \lesssim I_s$, there are some differences between experimental and theoretical values; it reflects the fact that the two-level model is too simple for these cases. More precise theoretical description requires using the model of more than two energy levels and contains more parameters than are necessary for our experiment. As shown in Fig. 4-3, if α_1, α_2 and I_s are chosen appropriately as fitting parameters, the absorption curves calculated from theory describe the experimentally observed absorption curves very well. This is sufficient for our purpose.
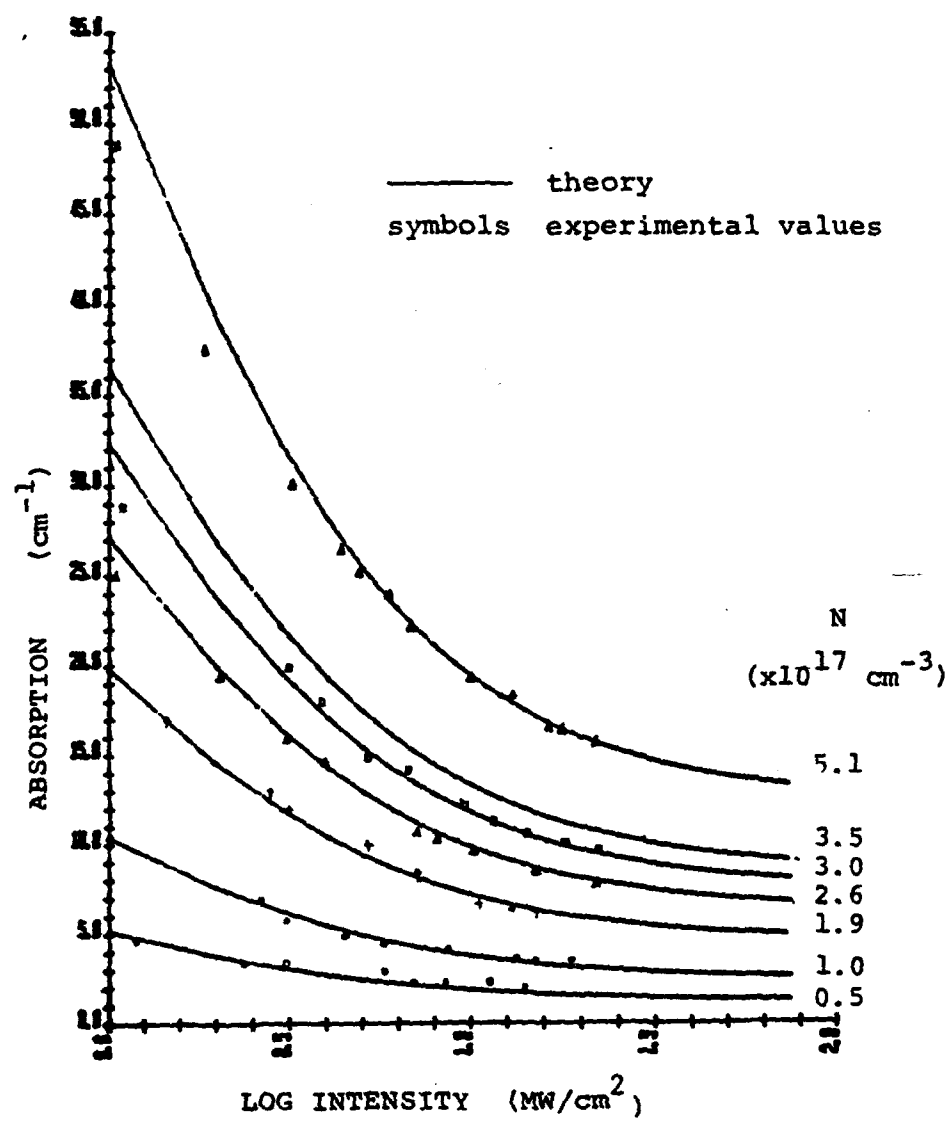
Figure 4-3. Plot of BDN dye absorption coefficient
as a function of incident light intensity.

IV.A-3 Bistable Characteristics of BDN

Our measurements for six BDN concentrations were made in the FP interferometer filled with BDN dichlorethane solution. BDN concentrations are $N = (0.5, 1, 1.9, 2.6, 2, 3.5) \times 10^{17} \text{cm}^{-3}$.

No bistability is observed experimentally for the former three lower concentrations as determined by the fact that the input and output pulses of FP interferometry are symmetric relative to their pulse peaks. Bistability is observed experimentally for the latter three higher concentrations. The obvious switch-on phonemena are observed from the oscilloscope traces. In Fig. 4-4 are shown three typical examples and the plots of I_{out} vs. I_{in} with time as a varying parameter, where for three concentrations the input intensities are normalized to the input peak intensity of 87.5 MW/cm^2, and the output intensities are normalized to the peak intensity of $N = 3.5 \times 10^{17}$ cm^{-3}. In order to estimate the experimental values of input pulse intensity and switch-on intensity I_{on} for three dye concentrations, we first fit the measured $I_{in}(t)$ by a Gaussian pulse and find the peak pulse intensity of $I_{in}(t)$ for each concentration. Then, we estimate I_{on} for three concentrations by comparing the corresponding values of switch-on points on the plots of I_{out} vs. I_{in} with the peak intensities of input pulses. We compared these experimental results to those theoretically predicted from the theory of the saturable absorber NLFP. We found that in order to fully explain the experimental results, it is necessary to include a nonlinear refractive index as well as a saturable absorption as a model for the dye, BDN. The validity of this assumption is found in the fact that four wave mixing has been observed in BDN. We were able to obtain a model which explained the experimental results, but further experimentation is required to confirm the validity of the theoretical model.
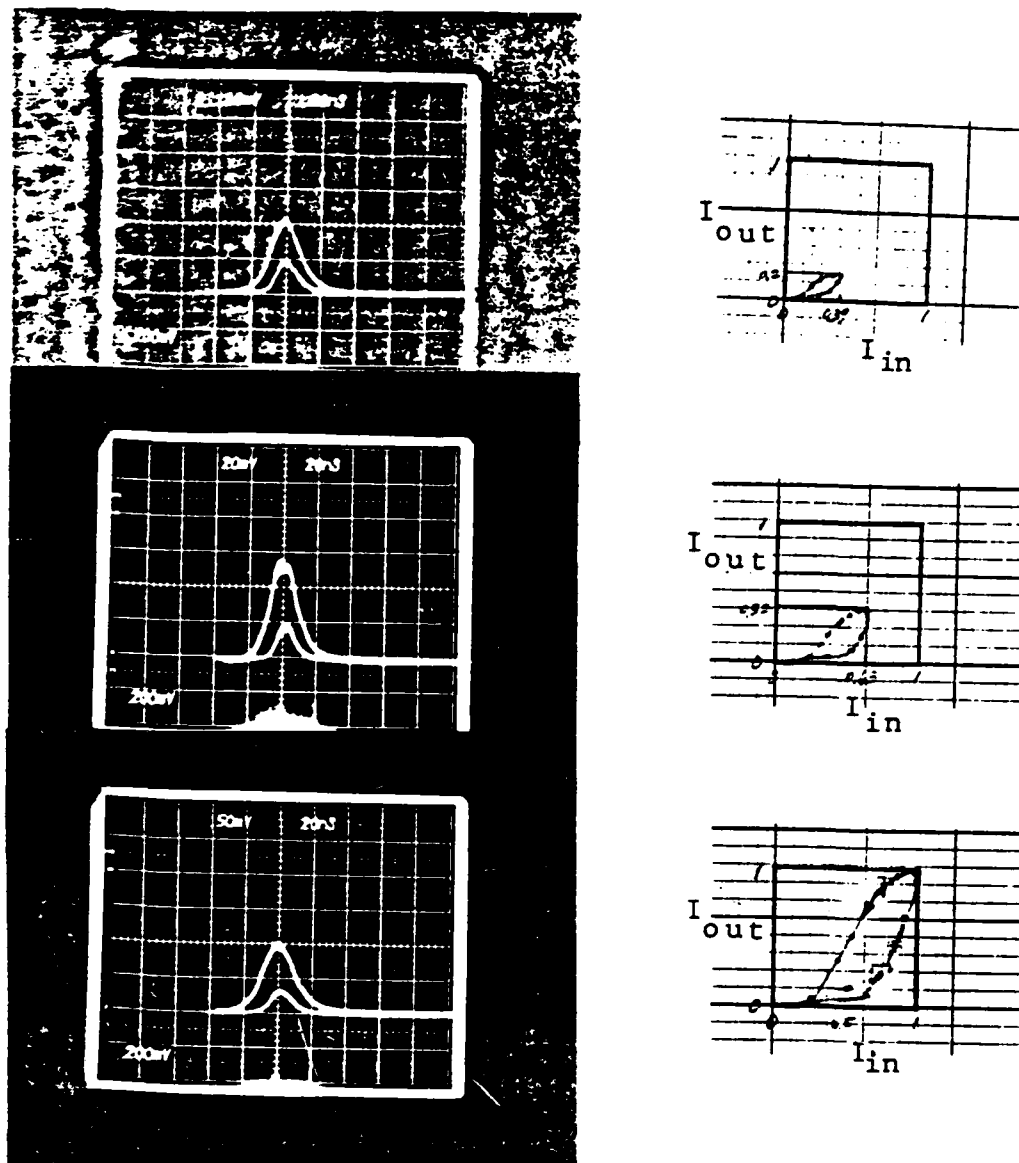
Figure 4-4.   Incident and transmitted intensity as
a function of time for three different dye concentrations,
Fabry-Perot aligned on resonance.   Transfer curves   determined
from point-by-point analysis of the oscilloscope curves are
plotted alongside the experimental data, showing hysteresis.
a) N = 2.6x10^{17} cm^{-3}.   b) N = 3x10^{17} cm^{-3}.   c) N = 3.5x10^{17} cm^{-3}.

IV.B Investigation of Optical Bistability in InAs

Optical bistability in semiconductors has been observed by Gibbs et.al. in GaAs (Appl. Phys. Lett. 35, 451 (1979)) and by Miller et.al. in InSb (Appl. Phys. Lett. 35, 658 (1979)). The nonlinearity responsible for the bistability observed in GaAs was attributed to a nonlinear index of refraction resulting from the saturation at high intensities of the absorption between discrete free exciton levels. The output from a dye laser was focused onto an epitaxially grown Fabry-Perot only 4 μm thick with R = 0.9 reflective coatings. With the laser tuned to a wavelength 10 - 25 Å longer than the exciton peak, bistability in the transmitted intensity was observed over temperatures ranging from 5°K to 120°K. The associated nonlinear refractive index n_2 can be estimated to be $n_2 \sim 10^{-7} cm^2/W$. The holding intensity was $1mW/\mu m^2$. The switch-on and switch-off times were <1 nsec and 40 nsec, respectively, with the longer switch off time reflecting the limitations imposed by the free exciton lifetime.

Miller et. al. measured bistability in a sample of n-type InSb, cut and polished plane parallel, 560 μm thick, with the natural reflectivity of InSb providing a measured finesse of 0.5. Using a CO laser line 100 - 200 Å below the conduction bandage at 5°K, bistability was observed. The associated nonlinear index can be estimated to be $n_2 \sim 5 \times 10^{-5} cm^2/W$, with a holding intensity of $0.02mW/\mu m^2$ at a spot size of 180 μm. The time constant associated with the effect remains to be determined. This group attributed the bistability they observed in InSb to a nonlinear refractive index resulting from the saturation of direct transitions between valence band and conduction band (Optics Comm., 27, 133 (1978)).

Although the mechanisms describing the optical nonlinearities differ, the results leave little doubt that semiconductors can provide the large optical nonlinearities and miniaturization capability required for practical all-optical bistable devices. We have begun a program this past year on InAs which is

directed toward generalizing the present understanding of the mechanisms responsible for the observed optical nonlinearities.

The exciton nonlinearity is fairly well understood. Gibbs et. al., prior to the bistability experiment, had shown that saturation of the well-known exciton absorption peak in GaAs was Bloch-like with an accompanying unsaturable loss term (Solid State Commun. 30, 271 (1979)), and that, consistent with earlier reports, the saturation intensity was quite low. Although the background unsaturable loss proved to be too large for absorptive bistability, dispersive bistability was achieved since the strong exciton resonance enhanced the nonlinear index.

The extent to which excitonic effects play a role in semiconductors with a smaller bandgap is not clear. Miller et.al. pointed out that it is unlikely that bound exictons would exist in their samples of InSb, due to the shielding by free carriers. However, remnant electron-hole interaction could be sufficient to affect the shape and location of the bandedge and thereby play a role in the effect. In the case of InAs, with an effective mass for conduction band electrons of $m^* = 0.03 \, m_e$, the free carrier densities for which screening will prevent bound excitons from existing is $N \geq 6 \times 10^{14} \, cm^3$. Since InAs with $N_D - N_A < 10^{16}$ is unobtainable at the present time, we do not expect a significant contribution from excitons.

The mechanism for the optical nonlinearity in InSb is not as well understood as that for GaAs. The theoretical model by Miller et.al., treated the direct transitions between the valence and conduction band as a collection of independent two-level systems. The intensity-dependent refractive index was attributed to the absorption of photons below the bandgap populating the conduction band, thereby eliminating their contribution to the resonance. The absorption of photons below the bandgap was attributed to band-tailing. The following expression for n_2 was derived:

$$n_2 = -\frac{1}{\hbar^3}\left(\frac{eP}{\hbar\omega}\right)^4 \frac{\tau}{T_2} \frac{2\pi}{15n^2c}\left(\frac{2m_r}{\hbar}\right)^{3/2}(\omega_G - \omega)^{-3/2}.$$

Here P is the matrix element connecting bloch states, τ a relaxation time, T_2 a dephasing time and m_r = the reduced mass. If one assumes that the values of P, τ, and T_2 are all close to those for InSb, then the relative magnitude of the effect would go as:

$$n_2 \propto \frac{E_g^{3/2}}{n^2\omega^4} \propto \frac{1}{n^2 E_g^{5/2}}.$$

The table shows the expected relative magnitude of n_2 predicted by this theoretical estimate for several direct gap III-V semiconductors.

TABLE Predicted nonlinear index in III-V Semiconductors

Semiconductor	E_G^* (eV)	n^*	$n_2/n_{2(InSb)}$
InSb	.18	4.1	1
InAs	.35	3.4	.3
GaSb	.78	3.9	3×10^{-2}
InP	1.35	3.3	10^{-2}
GaAs	1.43	3.7	7×10^{-3}

*Room Temperature Values

The nonlinear index in InAs is predicted to be only three times smaller than in InSb. Given Miller's estimate for InSb of $n_2 = 5 \times 10^{-5}$ cm^2/W, we expect the nonlinear index in InAs to be $\sim 10^{-5}$ cm^2/W. Using the above value of n_2, we can estimate the laser power required to cause bistability. The intensity available for bistability is limited by the minimum beam waist required to ensure that considerable beam expansion not occur while the beam is within the Fabry-Perot. The

condition that the bean waist, a, increase by <10% inside the
Fabry-Perot is

$$a \geq (5 L \lambda/n)^{1/2} F^{1/4}$$

where the finesse $F = 4R(1-R)^{-2}$. This defines the minimum
focusing area and maximum intensity available from a given
power, P. The observation of bistability requires that the
intensity be sufficiently large that the round trip phase
change inside the Fabry-Perot due to the nonlinearity, $\Delta\phi$,
be at least π. For a low finesse cavity, this leads to

$$P \geq \frac{\lambda^2 \pi \sqrt{F}}{3.2 \, n_2 n} \quad .$$

Notice that this condition does not depend on the length
of the Fabry-Perot, and that the higher the finesse, the more
incident power required to reach a phase change of π. On the
other hand, if the finesse is too low, a π phase change is
insufficient to cause bistability. Consider, for example, the
experimental results in InSb. Bistability was observed in
fifth order for a finesse $F = 0.5$.

Relating (2) and (4), we obtain the following anticipated
wavelength dependence for the required power:

$$P \propto \lambda^2 E_g^{5/2} \propto \lambda^{-1/2}$$

Thus the power requirements at 3 µm are only 30% higher than
those at 5 µm. The lowest intensity level at which Miller et.
al. observed bistability was 500 mW in an area 180 µm in dia-
meter. Since their Fabry-Perot had a length of 560 µm,
Eq. (3) shows that the minimum beam diameter that they could
have used would have been 50 µm. Focused to such a diameter,

an incident power level as low as 40 mW would have caused bistability since it would result in the same intensity level. An equivalent geometry at 3 μm would have a power threshold <55 mW.

The band gap of InAs lies near 3 μm which is within the range of the HF laser; consequently, much effort in the past year has been put into upgrading the HF laser that we have here at CLS. A new chemical ($NaOH/H_2O$) scrubber was built to handle the exhaust of the laser, replacing an inadequate dilution system. Improvements on the laser high voltage power supply were made by introducing a low pass filter between the power supply and laser to eliminate the 5%, 360 Hz voltage ripple that had been manifesting itself as a 20% ripple on the laser output. The laser resonator which had been designed for multiline operation was altered to allow insertion of a diffraction grating output coupler. As a result, single line – single longitudinal mode output was achieved at 14 wavelengths from 3.05 μm to 2.67 μm with single line powers as high as 3W.

InAs samples were obtained from Crystal Specialties Inc. of Monrovia, CA. Hall measurements were taken on the samples to determine carrier concentrations. The material was p-type with concentrations of $N_A - N_O \simeq 7 \times 10^{16} \mu m^{-3}$. Transmission measurements of the sample were taken on a spectrophotometer to determine the location of the band edge of the sample. In Fig. 4-5 are plots of absorption coefficient versus photon energy for our sample at 300°K and 77°K along with data for an n-type sample from Dixon and Ellis (Phys. Rev. 123, 1560 (1961)). The range of the HF and DF laser lines are indicated. The two horizontal lines indicate the range of absorption coefficient over which the nonlinearity in InSb has been observed.

The consequences of the impurities in our sample are two fold. First, the horizontal shift of our p-type sample data at 300°K relative to the n-type data of Dixon and Ellis is indicative of the dependence of the band gap to impurity type. It has been shown that the band edge will shift to lower or
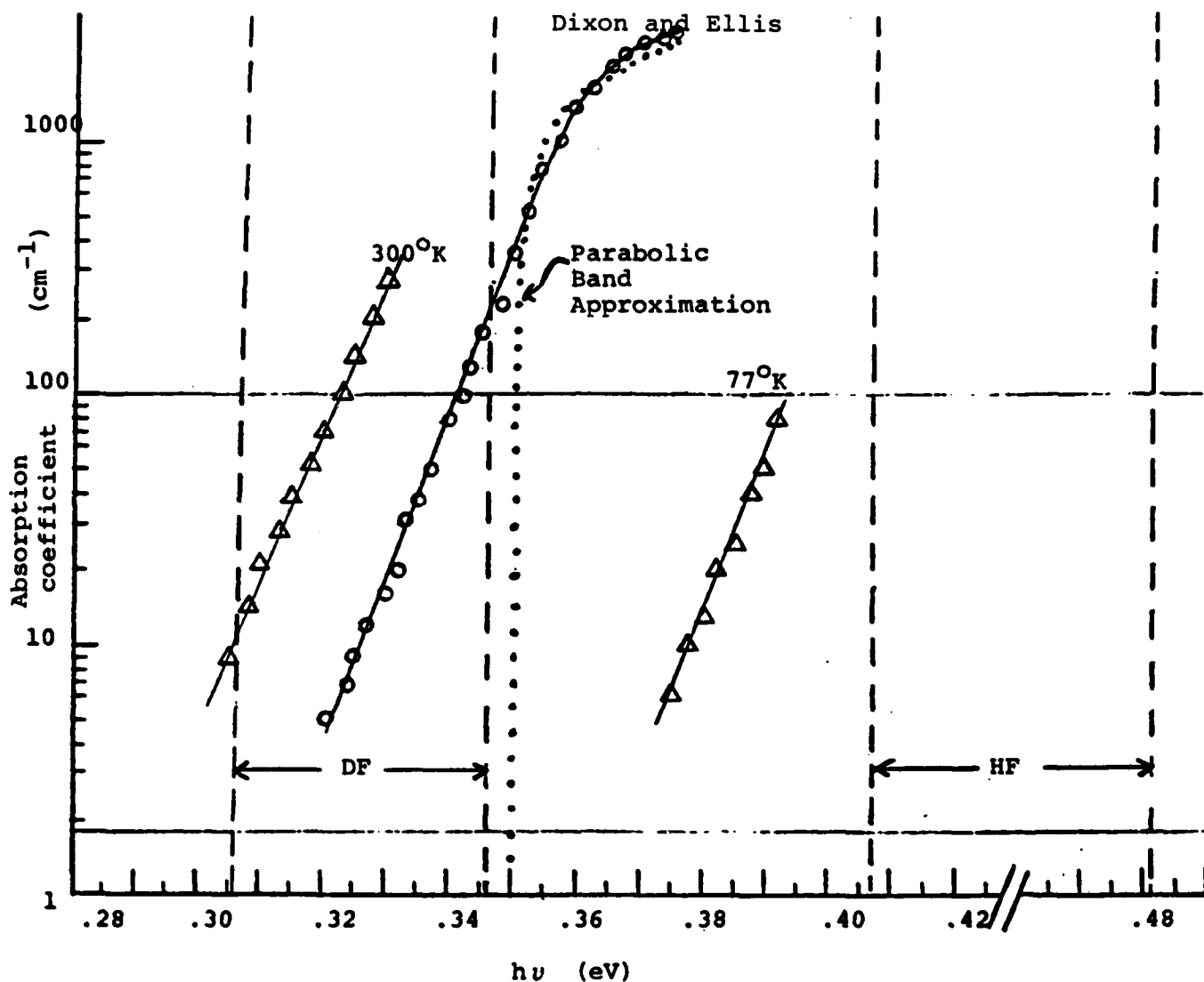
Figure 4-5. Absorption coefficient vs. photon energy for the experimental p-type sample and an n-type sample taken from the literature. Vertical dashed lines indicate range of HF and DF laser lines. Horizontal lines indicate range of α in which nonlinearity experiments were carried out in InSb.

higher energy depending on whether the material is p-type or
n-type with the magnitude of the shift being related to the
amount of impurity (E. Burstein, Phys. Rev. 93, 632 (1954)).
Dixon and Ellis had observed this in InAs also.

This shifted our sample out of the range of the HF laser
lines although at room temperature it is well within the DF
band. Operating the laser in the DF mode with the sample at
room temperature has several disadvantages. Unfortunately the
power output on the DF lines is necessarily much less, due to
lower gain, and we were not able to obtain sufficient power.
Secondly, at room temperature we anticipate absorption by
impurity levels to be significant. One way of reducing such
absorption is to reduce the temperature of the sample so that
fewer impurity levels will be unoccupied and able to contribute
to the absorption.

The second consequence of impurities is that the band edge
is less abrupt, with absorption extending well into the band
gap. This is evident in Fig. 4-5 where we have shown the para-
bolic band approximation fitted to the data of Dixon and Ellis
using the quoted value of the band gap for their sample
(.35 eV). In using the parabolic band approximation, one uses
the fact that absorption in a direct gap semiconductor goes as

$$\alpha \ (h\nu) \ \propto \ (h\nu \ - \ E_G)^{\frac{1}{2}}$$

Determination of the band gap is obtained by plotting α^2 vs. $h\nu$
with the interception the energy axis yielding E_G. When impur-
ities are involved, such a plot yields a straight line only for
large values of α, where absorption by impurity levels is neg-
ligible. In the case of Dixon and Ellis, a straight line was
obtained for values of α above $10^3 cm^{-1}$. By extrapolating this
line to zero absorption, they obtained their value of .35eV.
But as can be seen, absorption continues well below the band
gap. This effect, which tends to smear out the bandgap and
also the resonance that gives rise to the nonlinearity we hope

46

to see, may be a problem at the higher temperatures even with the most pure. InAs samples available (N_d-N_A~10^{16}cm^{-3}). At low temperatures we expect it will be greatly diminished. Future plans are therefore to:

1) Improve the DF mode of operation of our laser to allow investigation of optical nonlinearities in InAs at room temperature.

2) Obtain n-type samples of greater purity (~2 x 10^{16}cm^{-3})

3) Expand the range of sample temperature by going to a liquid helium dewar in order to bring the sample within range of the HF laser lines and decrease impurity effects.

IV-C. THEORY OF BISTABILITY IN NONLINEAR DISTRIBUTED FEEDBACK STRUCTURES

It has been established theoretically and experimentally that a Fabry-Perot interferometer filled with a non-linear index medium exhibits hysteresis and bistability in its response to optical inputs. Such a device has potential applications as an optical transistor, pulse shaper, memory element and differential amplifier. The underlying physical requirements are an intensity-dependent refractive index and an optical feedback mechanism. Previous theory and experiments on optical bistability have employed systems with lumped feedback; i.e., the feedback mechanism is spatially localized at the ends of a homogeneous nonlinear medium either as mirrors or Bragg reflectors . In this study we developed an exactly solvable model of bistability in a device in which the feedback mechanism is distributed throughout the nonlinear medium as a periodic variation of the linear refractive index.

The nonlinear distributed feedback structure (DFB) has a threshold for bistability which is comparable to the Fabry-Perot structure (FP) and has several distinct features. These include the possibility of a truly bistable device (FP devices are all multistable), absence of the strong optical limiting seen in FP's (except for DFB's with very large coupling coefficients), a decrease in optical hysteresis width with increasing input intensity, and the characteristic monochromatic spectral response of DFB structures. In addition to its obvious compatibility with integrated optics, the DFB bistable device offers the advantage of control over the input/output characteristics by tailoring the DFB transmission

48

through tapering the coupling strength or chirping the frequency of its grating.

The theoretical analysis of the non-linear DFB structure led us to consider that since a four-wave mixing structure has the same basic geometry, it should also exhibit bistability. The object of this study was to point out some new effects which can occur in degenerate four-wave mixing processes. In particular we show that the intensity-dependent refractive index leads to hysteresis and optical bistability when the intensities of the interacting waves are sufficiently high. The effects described here do not depend on external resonant cavities, in contrast to the nonlinear Fabry-Perot devices.

The degenerate four-wave mixing process (DFWM) can be regarded as the formation and reading out in real time of a thick holographic grating. A probe wave interferes with the counterpropagating pump beams. Through the intensity dependent refractive index a phase grating is created which then diffracts the other pump beam to generate a signal wave. As in the DFB structure, bistability then results from the intensity-dependent Bragg condition for coupling between the interacting waves. Because the DFWM process is capable of gain and oscillation[4] othertypes of bistable behavior are available here which cannot be found in the passive DFB structure. Specifically an oscillation hysteresis is shown to be possible.

By using the slowly varying envelope approximation, we found it possible to solve the exact coupled wave theory, taking into account propagation effects. The results have already been published. "Theory of Bistability in Nonlinear Distributed Feedback Structures" by Winful, Marburger and Garmire was published in Applied Physics Letters 35 379 (1979). "Hysteresis and Optical Bistability in Degenerate Four-Wave Mixing" by Winful and Marburger was published in Applied Physics Letters 36 613 (1980). Further details are available in the thesis of Herbert Winful, Department of Electrical Engineering, PhD, 1981.

V.   TRANSIENT PHENOMENA IN BISTABLE DEVICES

We have undertaken a three-year research program on trans-
ient phenomena in bistable optical devices. We have considered
both Fabry-Perot interferometers with nonlinear media inside
the cavity, and hybrid electrical-optical devices, in the
regime in which the response time of the nonlinear medium is
either equal to or much longer than round trip time of the
cavity. These studies resulted in a number of publications,
and several new effects, as well as several additional new
ideas, which are currently being explored. In this section,
we outline each of these new effects and describe which ones
will be useful in optical signal processing. While the treat-
ment here considers single elements, all the results apply
equally well for image processing.

V.A Critical Slowing Down

The first new effect is "critical slowing down". This is
a nonlinear delay in switching time which occurs when the
switching signal is only very slightly larger than the cri-
tical value required by the steady-state theory. Critical
slowing down is a well-known effect in many nonlinear systems,
and occurs because of the fact that the nonlinearity itself
causes the switching. The closer the system gets to the
critical point for switching, the smaller the impetus given to
switching from the nonlinearity. In the limit of switching
exactly at the critical intensity, I_c (as determined from
steady-state analysis), the driving term becomes infinitely small
and the switching time goes to infinity. Critical slowing down
commonly occurs in other nonlinear systems, as for example, in
phase transitions.

How big the effect is depends on the details of the bistable
system. We carried out a detailed study of critical slowing down
in the hybrid bistable device, observing it experimentally and
finding good agreement with theory, (Garmire, Marburger, Allen,
Winful, Appl. Phys. Lett. 34, 374 (1976)). The results are shown
in Fig. 5-1, demonstrating the increase in switching time at
small switching signals. It can be seen that inputs greater
than twice the steady-state switching intensity are needed to
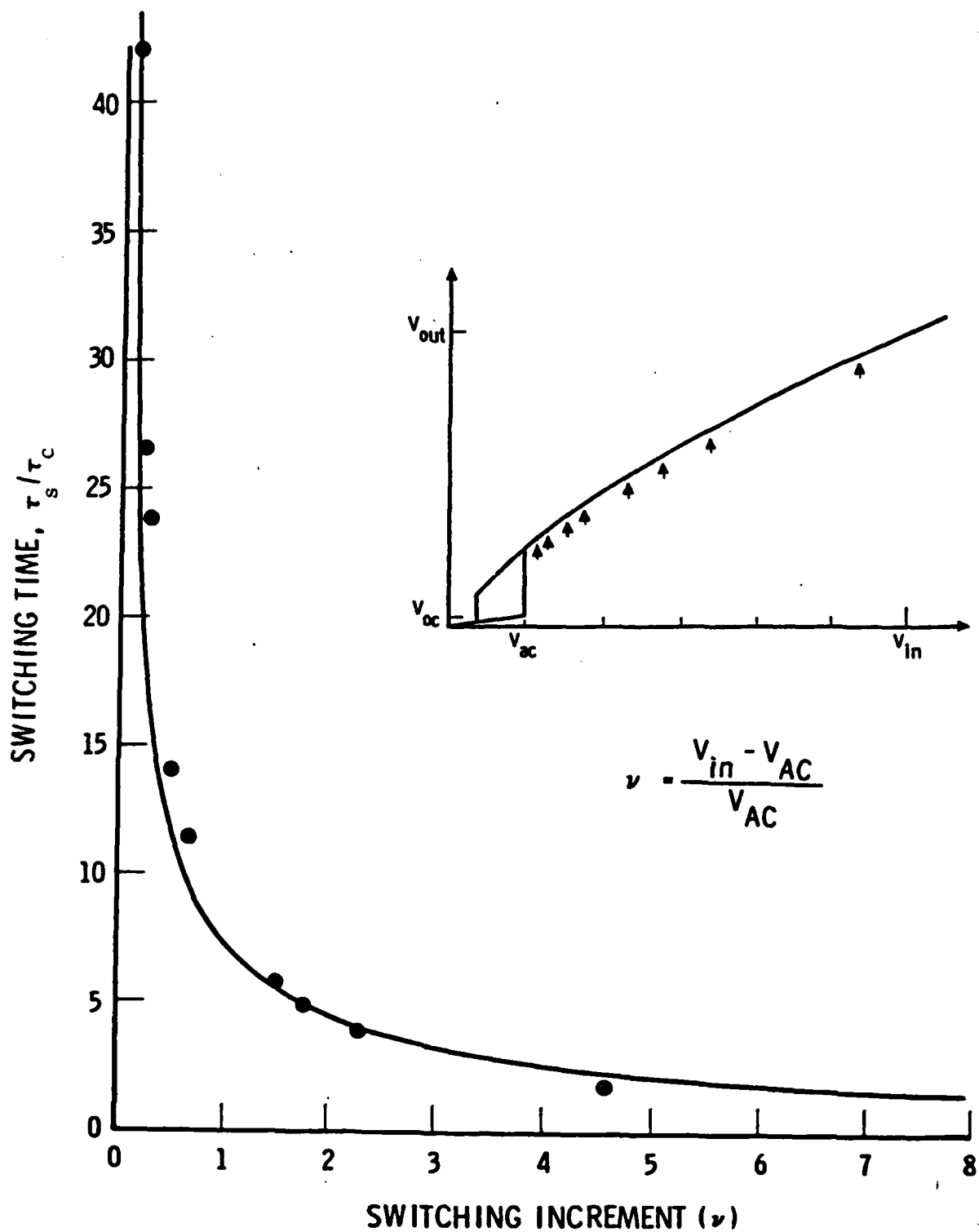
Figure 5-1. Plot of response time of a bistable device to a step-input signal as a function of the fractional increase in input over critical incident signal, V_{AC}.

Inset shows the experimental bistability curve and defines the critical incident signal, V_{AC}.

$$\nu = \frac{V_{in} - V_{AC}}{V_{AC}}$$

observe switching times shorter than four times the response
time of the device.

We have derived a simple equation for the switching time of
a bistable device. When the medium response time is much longer
than the cavity roundtrip time, transient response of the bi-
stable device can be modeled by a single first order differential
equation:

$$\tau_c \frac{\partial I}{\partial t} + I = I_o T(I) \qquad (5\text{-}1)$$

where I_o is the incident light level and I is the transmitted
light. $T(I)$ is the transmission of the bistable device (for
example, a nonlinear Fabry-Perot) expressed as a function of
the output intensity. When a hybrid bistable device is con-
sidered, the same equation applies if the light levels are mea-
sured in voltage units. We have solved Eq. (5-1) for step
increments in incident light. We obtained an analytic express-
sion for the switching time τ_s as a function of switching
power for any bistable device:

$$\tau_s / \tau_c = 2\pi\nu^{-\frac{1}{2}} \{A(1+\nu) - \nu\}^{-\frac{1}{2}} \qquad (5\text{-}2)$$

where ν is the fractional increment the incident signal is
above the critical intensity, $\nu = (I - I_c) I_c$, and τ = the
lifetime of the nonlinear medium. A is the parameter of the
bistable device: $A = 2 I_c I_{oc} (\partial^2 T / \partial I^2)_{oc}$, where I_{oc} is the
output signal at the critical incident intensity, just before
switch-on, and the last factor is the second derivative of the
transmission with respect to intensity, expressed at I_{oc}.
Equation 5-2 is the theoretical curve which is plotted in
Fig. 5-1 for the hybrid device, where $T(I) = \frac{1}{2}(1 - F \cos(I + V_B))$.

We have also calculated Eq. (5-2) for the nonlinear
Fabry-Perot in which $T(I) = (1 + F \sin^2(I - \theta_o))^{-1}$. In Fig. 5-2
we show some general NLFP results. In particular, we have
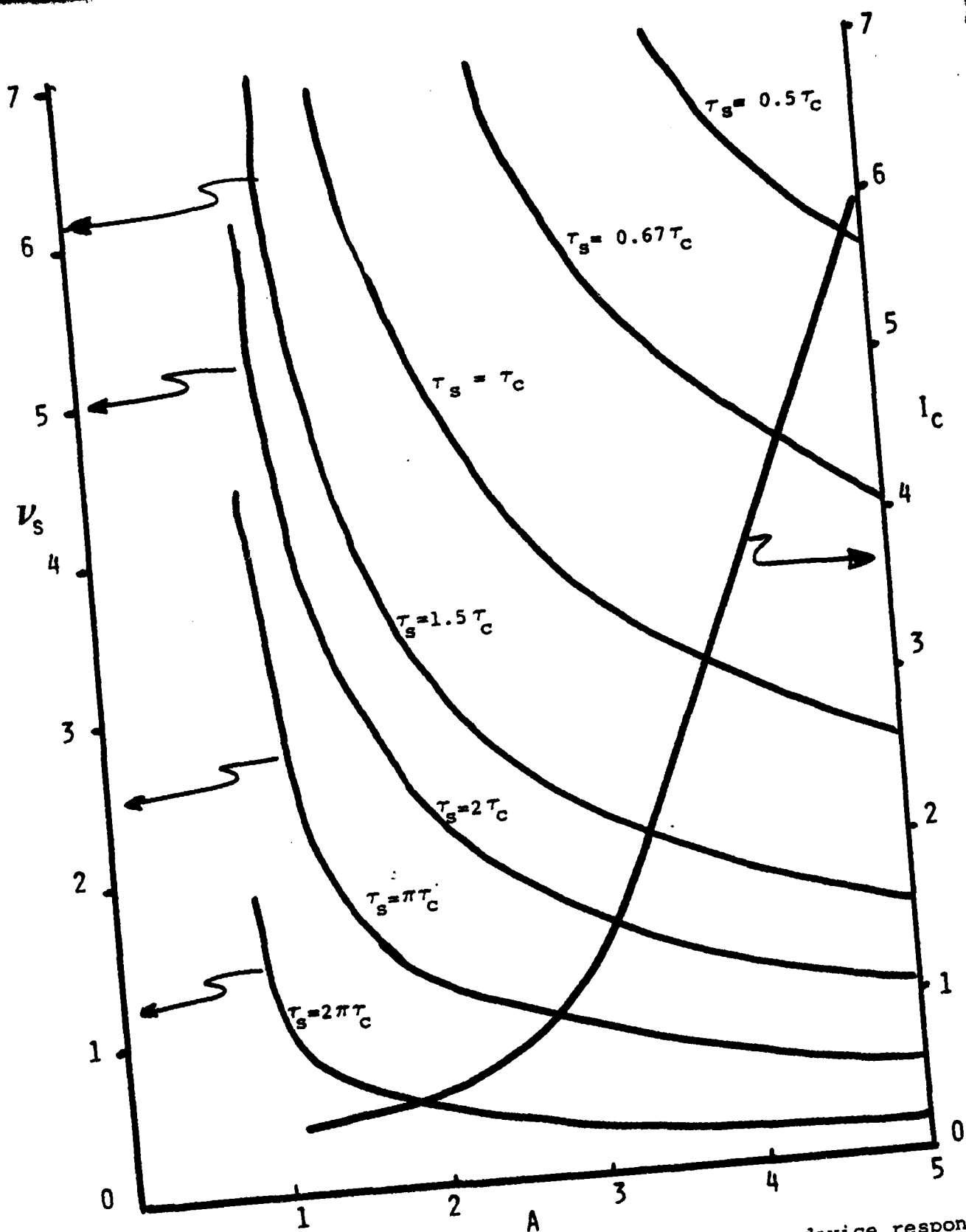calculated the value of the increment ν_s required to achieve a

Figure 5-2. Switching increment ν_s which causes a device response time τ_s as a function of the bistable device parameter A. Also included is the critical incident intensity I_c required in steady-state operation.

54

response time τ_s for the device, as a function of the parameter A (which depends on the NLFP phase bias for a given finesse). As long as the incident light level is such that $\nu > \nu_s$, then the device response time is no greater than τ_s. It can be seen that larger values for A give smaller values for ν_s, which means that the incident light intensity does not need to be as far above I_c to ensure switching in a time less than τ_s. Increase in the value of A for a NLFP is obtained by operating very near to resonance, at the low intensity limit. Values for A may increase to anywhere from 10 to 1000. For these large A values, critical slowing down is not a problem. However, we also show in Fig. 5-2 that utilizing larger A increases the incident intensity required to cause bistability, I_c. Thus, in any given system, there is a trade-off between incident intensity and response time. The value of A will be determined by the system requirements.

Notice that for A = 2, at incident light levels 50% above I_c ($\nu = 1.5$), the device response time is approximately 2π times the nonlinear medium response time. It requires incident light level of more than three times I_c to obtain switching in only twice the nonlinear medium response time. In fact, the device response time equals that of the medium only when the incident intensity is more than six times the steady-state value for the critical intensity. Notice that for sufficiently high intensities, it is possible to obtain switching in a time faster than the medium response time, although this is unlikely to be a useful mode of operation because of the very large intensities required.

Critical slowing down has important implications for the observation of bistability using short pulses in media whose response times are not sufficiently fast. The bistable device response time will typically be about six-times slower than the nonlinearity of the medium. This means that the incident light pulse must be at least six times longer than the response time of the nonlinear medium. When this condition is not satisfied, the apparent threshold for bistability will be increased, due

to the requirement for higher incident light levels to shorten the switching time. The value for A is strongly dependent on how close the linear Fabry-Perot is to resonance with the incident light. Since this resonance is strongly dependent on experimental factors such as temperature, the switching time will also be strongly dependent on experimental factors.

Critical slowing down has impact also on the calculation of the switching energy of a bistable device, which is normally considered to be the product of the switching intensity times the effective switching time. We have shown that the switch energy is

$$E = 2\pi \ (A - 1)^{-\frac{1}{2}} \ I_s \ \tau_c \quad .$$

When A = 2, the bistable device switch energy is typically two times the product of the switching intensity and nonlinearity response time. This higher switch energy must be taken into account when designing bistable devices operating in the pulsed mode.

In addition to critical slowing down occurring when switching the device up to its final state, critical slowing down also occurs when switching down to a level just below the minimum holding energy. Experimental examples of critical slowing down during a down-switch in a hybrid device are shown in Fig. 5-3.

V.B Pulse Shaping

In the last section we considered critical slowing down as a problem which must be overcome in order for the switching of a bistable device to be rapid. In this section we point out that with proper control of incident intensity, it is possible to "shape" a pulse by using critical slowing down to delay the onset of pulse. We demonstrated this effect with the hybrid device, shown in Fig. 5-4. In this case a square pulse was essentially reduced in width a factor of two by critical slowing down.

The transient shape of the output in a bistable device is often dominated by one or more peaks which occur because the device
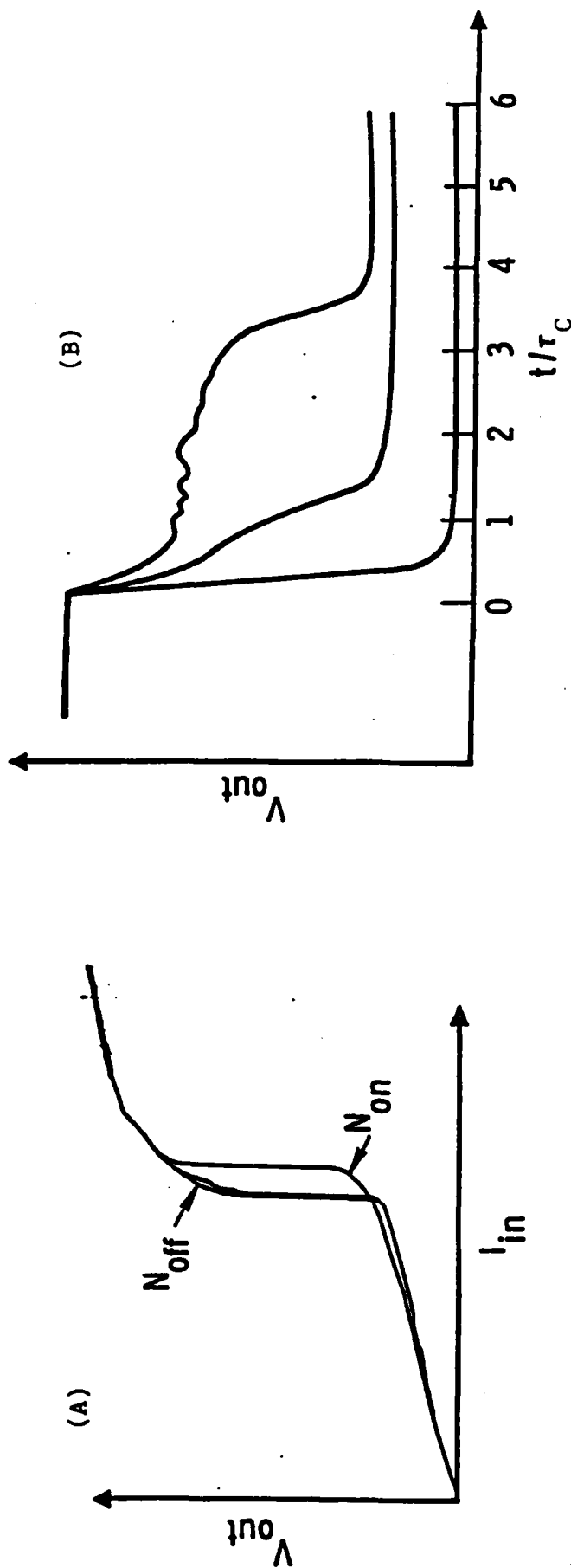
Figure 5-3. Experimental data from hybrid bistable device on critical slowing down during down-switching. A) Steady-state transfer curve; N_{on} and N_{off} are the intensity levels at which the device sits for the longest time during critical slowing down. B) Transient response of the bistable optical device from a steady-state output in the high stable state to different lower steady-state intensity levels. Note that the higher the intensity in the off-state, the slower the transition. The two figures have the same vertical scale.

EXPERIMENTAL RESULTS

STEP INPUT
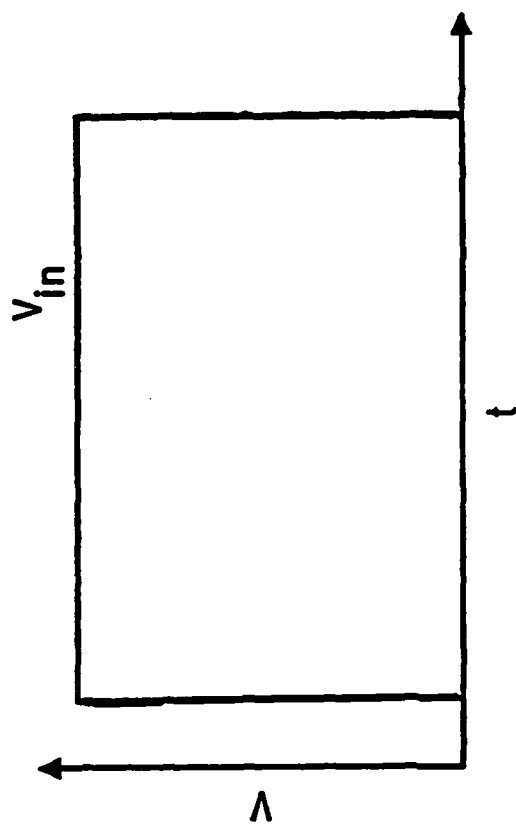
TRANSIENT RESPONSE
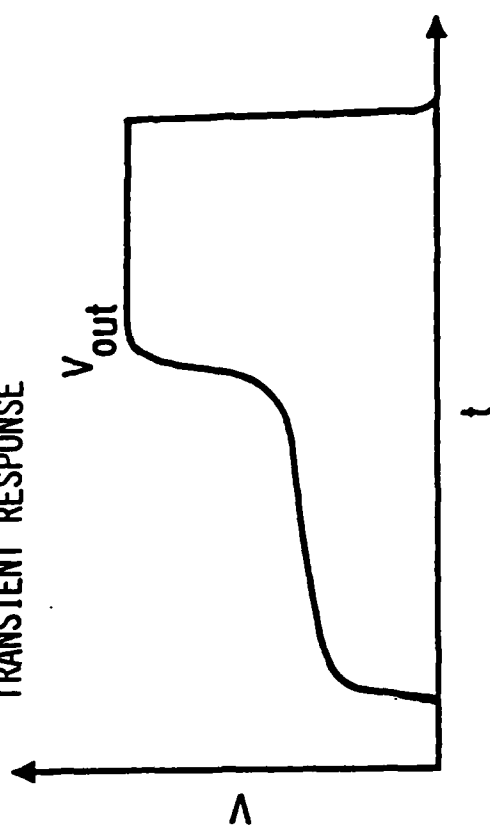
TRANSFER CURVE
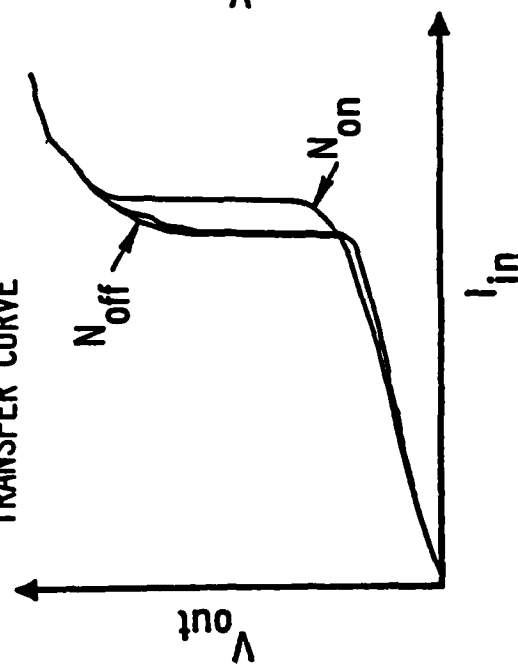
Figure 5-4. Experimental results with hybrid BOD for pulse shaping of a square pulse. The long delay from critical slowing down occurs at N_{on} and causes an effective pulse shortening.

58

rapidly passes through the maxima in its transmission function. Consider, for example, the hybrid device. If the voltage across the modulator is monitored, these peaks are not observed, because the time-constant of the electronics creating the voltage is slower than the time it takes the light to respond to the changes in the modulator transmission function. If, however, the light output is monitored with a fast detector, we observe these transient peaks which result from the device rapidly passing through its transmission peaks. A typical experimental result is shown in Fig. 5-5.

Similar behavior has been seen in our numerical studies of the nonlinear Fabry-Perot. Figure 5-6 shows a typical numerical example for a Gaussian input pulse. The several spikes corresponds to the fact that the NLFP is being excited up to its fourth stable state.

V.C Overshoot Switching

In the course of our study on transient effects in bistable devices, we realized that several new effects were possible when the devices have two comparable time constants. The first of these we have termed "overshoot switching".

Overshoot switching is a transient switching phenomenon which occurs when the bistable device has two time constants which are within an order of magnitude of each other. The origin of this effect lies in the fact that an abruptly changing input signal causes overshoots in the response of the medium. When these overshoots are sufficiently large, and occur in times comparable to the round-trip cavity time, they may cause switching to the upper state, even when the incident light level is below that which would cause switching by steady-state considerations.

Overshoot switching is most easily understood by considering the hybrid BOD. The transient response of the hybrid bistable device with two time constants can be described by a single, second order differential equation:

$$\tau_1 \tau_2 \frac{d^2 I}{dt^2} + (\tau_1 + \tau_2) \frac{dI}{dt} + I = I_o \, T \, (\gamma I) \tag{5-3}$$
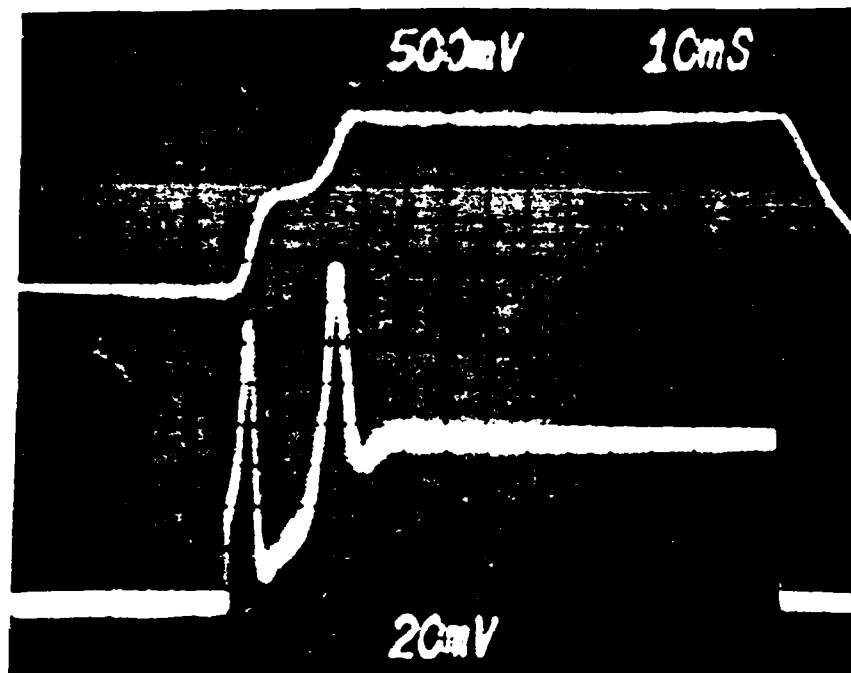
59

Figure 5-5. Experimental output from the hybrid bistable device as a function of time. The top trace is the voltage across the modulator. The bottom trace is the light output as a function of time.
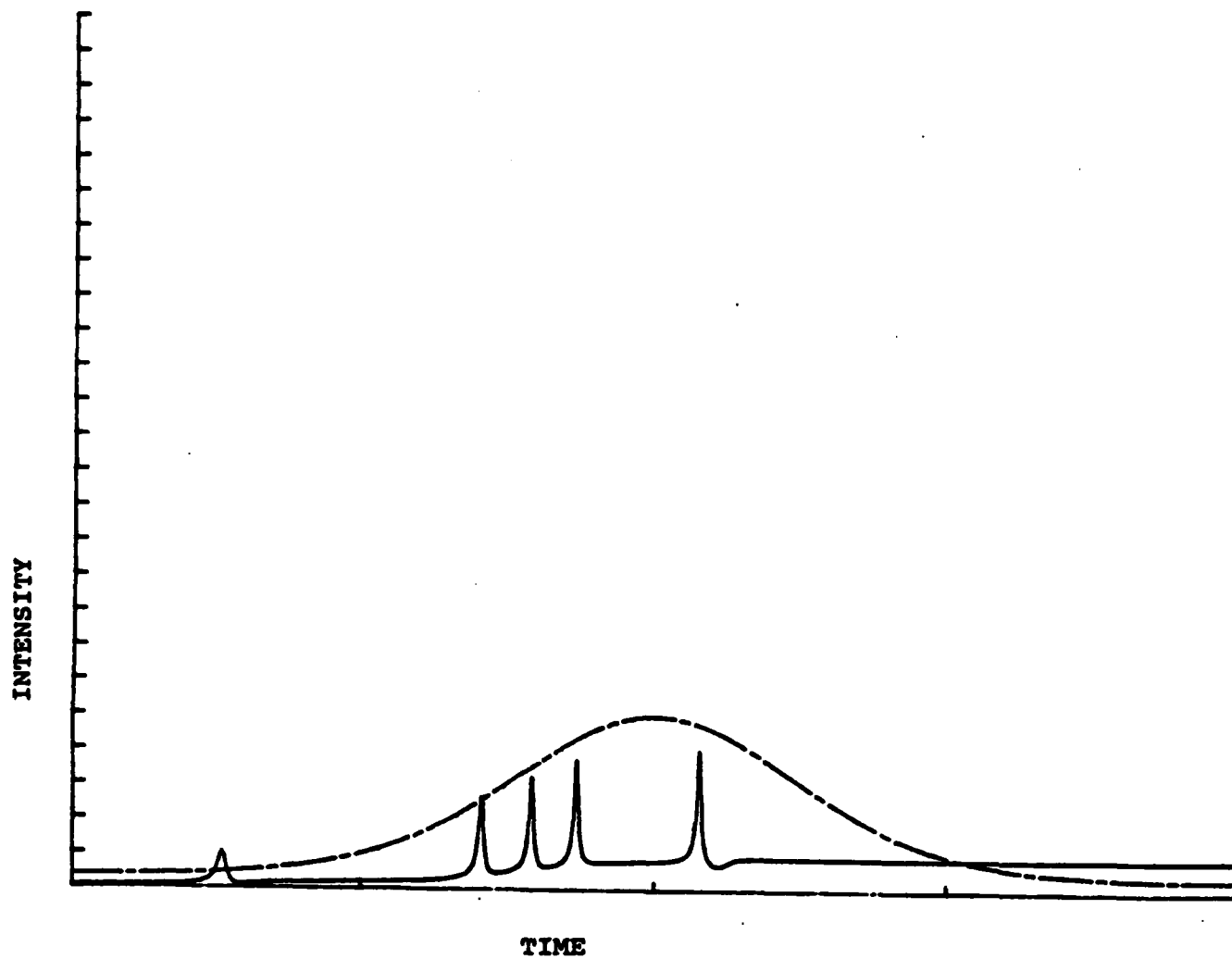
Figure 5-6. Numerical solution to the transmission of a non-linear Fabry-Perot as a function of time for a Gaussian input pulse.

61

where τ_1 and τ_2 are the two response times of the system. I_0 and I are the incident and transmitted light power, T is the transmission of the hybrid modulator, and γ is the amplification factor expressed as a ratio of the voltage across the modulator to the transmitted light power. From the form of this equation it is possible to make the analogy with a particle in a potential well and to understand overshoot switching as the fact that sufficient momentum will carry a particle over a local potential minimum into a separate potential well (stable state). This overshoot causes switching from the lower into the higher stable state of the hybrid device as incident signal levels as much as 30% lower than the critical value, I_c. Figure 5-7 shows the experimental and theoretical results for a $LiNbO_3$ hybrid modulator (Goldstone, Ho and Garmire, Appl. Phys. Lett. 37 126 (1980)).

Overshoot switching also occurs in the nonlinear Fabry-Perot when the round-trip time in the NLFP is comparable to the response time of the nonlinear medium. We derived a set of coupled differential equations which are valid as long as the variations in input signal in one round trip time are small. The only regime in which these equations break down is when the round trip time is much longer than the relaxation time of the medium. These equations are (Goldstone and Garmire, IEEE J. Quantum Electro. QE-17 366 (1981)):

$$\tau_c \frac{\partial E(t)}{\partial t} + \{1-Re^{i\phi(t)}\} E(t) = (1-R)E_0(t+\frac{\tau_c}{2}) \qquad (5\text{-}4)$$

and

$$\tau_n \frac{\partial \phi}{\partial t} + \phi = \phi_0 + \beta |E(t)|^2 \qquad (5\text{-}5)$$

where $E(t)$ and E_0 are the transmitted and incident fields, respectively, ϕ is the round trip excess phase change due to the nonlinearity, ϕ_0 is the linear cavity roundtrip detuning, R is the reflectivity of each mirror, τ_c and τ_n are the cavity round trip time and medium response times, respectively, and β is a constant proportional to the nonlinearity.
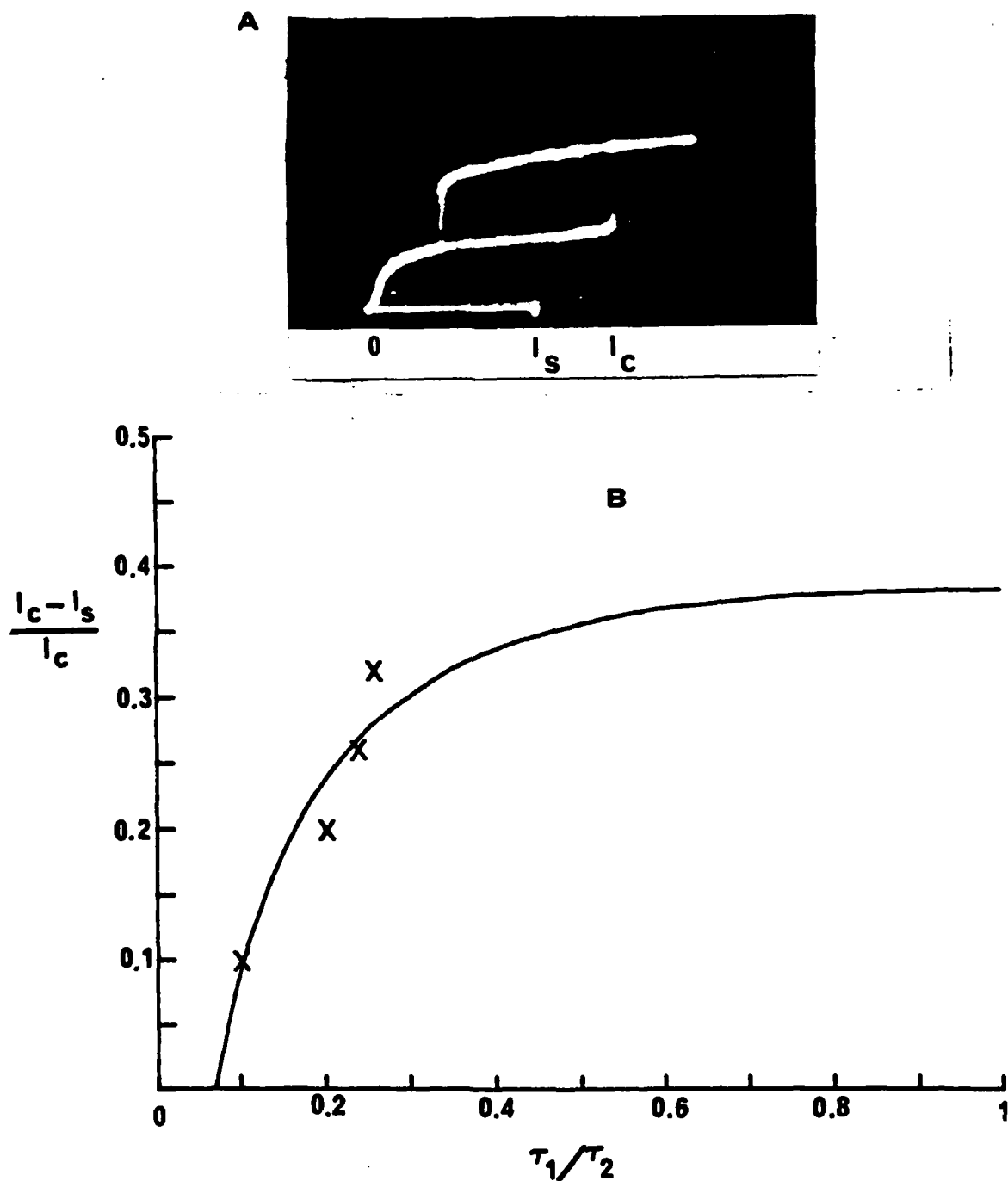
Figure 5-7. Experimental results on overshoot switch in a hybrid BOD. a) experimental transfer curve b) fractional increment switching occured below ss value as a function of the ratio of the device time constants.

From numerical solutions to these equations, we have determined that overshoot switching does indeed take place. Just as in the case of the hybrid, the amount below the incident critical intensity at which steady-state switching takes place depends on the ratio between the two time constants. Figure 5-8 shows the result of numerical integrations of equations 5-4 and 5-5. Note the similarity of the NLFP to the hybrid. The size of the effect is comparable that observed in the hybrid. In the NLFP, however, the equation is not exactly symmetric in the two time constants. It should be noticed that the maximum effect is less than 30%, so that overshoot switching may be difficult to observe directly in physical systems. However, it leads to several new effects which would not be observable without the existence of overshoot switching which are described in the following sections.

In addition to overshoot switching, it should be pointed out that there is a comparable effect, termed "undershoot" switching which occurs when the signal is abruptly reduced in intensity. "Undershoot switching" means that the reduction need not be sufficient to take the device below its holding intensity, but that abrupt reduction to intensity levels roughly 30% higher than the minimum holding intensity will cause the device to overshoot and switch down to the lower state.

The "abruptness" is an important part of the existence of overshoot switching. We will show in a later section that if the pulse risetime is sufficiently slow, overshoot switching will not take place. First, however, we describe an interesting effect due to overshoot switching which unambiguously proves its existence -- alternate switching.

V-D Alternate Switching

The phenomenon of alternate switching occurs when the bistable device is subject to a train of pulses and is operating in the overshoot switching regime. The bistable device keeps a memory of the last state in which it found itself for times comparable to the longest time constant in the system - here
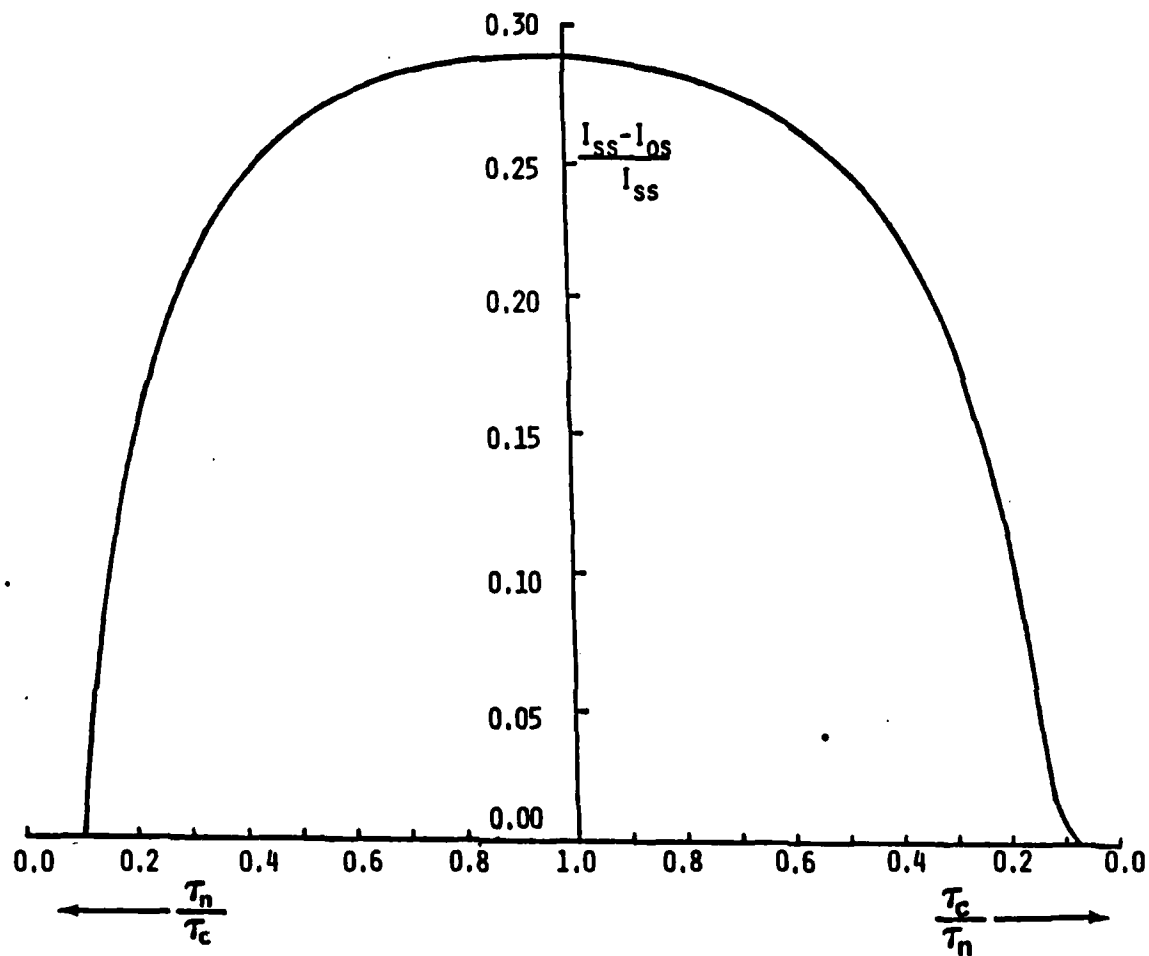
64

Figure 5-8. Fraction below critical incident steady-state intensity that bistable device switches, as a function of ratio of time constants.

assumed to be the response time of the nonlinear medium. If
the device is switched off and then on again, the new state
will depend on how long the device was off.

Four regimes of off-times can be identified. For the
longest off-times, the pulses act independently. If the first
pulse causes overshoot switching, each successive pulse also
causes overshoot switching and the device is always found in
the higher state. If the time between pulses is shortened,
the response of the bistable device does not fully decay
before the next pulses arrives. In this case there is not suf-
ficient "momentum" provided by the second pulse to cause the
device to overshoot into the higher state during the second
pulse. As a result, while the output corresponding to the
first pulse was in the high state, the output of the second
identical pulse is in the low state. During the off-time
after the second pulse, the bistable device transient response
decays to a value lower than it did after the first pulse,
since it was in the low state at the start of the off-time.
If the off-time is sufficiently long, the final value may be
sufficiently low that the third pulse can provide sufficient
"momentum" to again cause overshoot switching, and the third
pulse will cause the bistable device to return to the high
state. In this way, alternating pulses of high and low states
are created. Experimental results of alternate switching are
shown in Fig. 5-9. The results have been fully explained by
theoretical analysis, and are outlined in a recent publication
(Goldstone, Ho, Garmire, Applied Physics Letters 37 126 (1980)).

If the off-time between pulses is shorter than that which
creates alternate switching, the bistable device cannot relax
after the second pulse far enough to again overshoot switch.
As a result, after a first high-state pulse, all successive
pulses correspond to the low state. This is the third regime
of operation. Finally, if the time between pulses is very short,
decay out of a state is not possible between pulses and the
device acts as a steady-state bistable device. In other words,
all pulses will be either in the high state or in the low
state depending on the initial conditions. The experimental
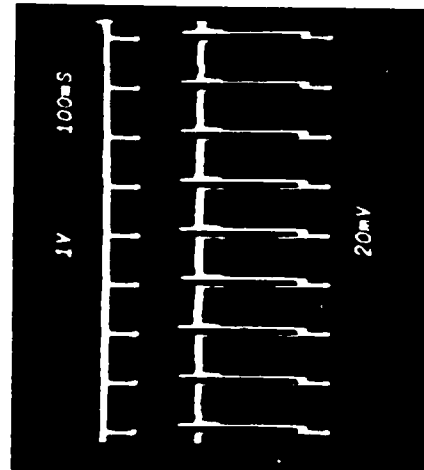results were obtained by biasing a hybrid bistable device in

66
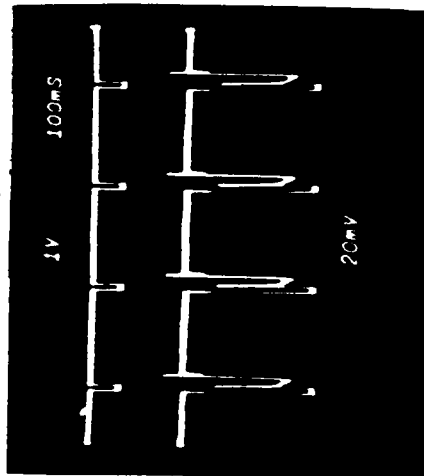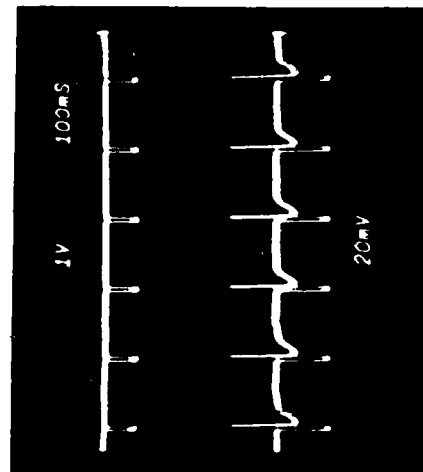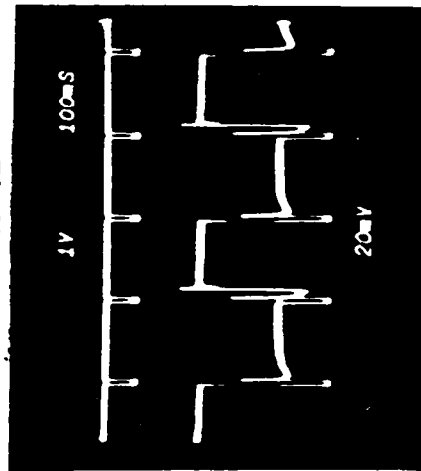
Figure 5-9. Four regimes of operation of a bistable optical device subject to a pulse train in the overshoot switching regime.

the overshoot switching regime and subjecting it to a stream of
pulses produced by a cw laser and a rotating chopper wheel. The
only change in the four photographs was the speed of the chopper,
creating different regimes of off-time. The numerical values
of off-times to create the different regimes were within 15% of
the theoretical values.

The NLFP also exhibits alternate switching and the four
regimes of off-times, when subject to a stream of pulses in
the overshoot switching regime. We have proved this by numerical
solution of Eqs. 5-4 and 5-5. The results are shown in a recent
publication (Goldstone and Garmire, IEEE J. Quantum Electr.
QE-17 366 (1981)). The behavior is essentially identical to
the hybrid experimental results, and therefore is not presented
here.

V.E Risetime Detection

It was mentioned in section V-C that overshoot switching
requires a rapid rise in the incident light signal. This is
because equation 5-3 represents a particle in a stationary well
only for suddenly switched-on constant incident intensity. The
"momentum" of the particle originates from the sudden change
in state of the potential well due to a sudden onset of the
incident light. If the incident light signal is switched on
gradually, the "particle" does not receive sufficient momentum
to propel it past the local minimum, over the local maximum
and into the next stable state. The observation of overshoot
switching, therefore, requires a sufficiently fast risetime.
Thus the bistable device, biased into the overshoot regime,
becomes a risetime detector.

We observed risetime detection in the hybrid bistable
device both experimentally and theoretically. We adjusted the
$LiNbO_3$ modulator hybrid bistable device to operate in the
overshoot switching regime for rapid-rise pulses. The system
was not changed in any way except to slow down the rise-time
of the incident light pulse. The result was to destroy over-
shoot switching, leaving the BOD in the ground state. This
effect was found experimentally and confirmed theoretically in
the hybrid BOD.

The same effect was found in the nonlinear Fabry-Perot by numerical integrations of Eqs. (5-4) and (5-5) for inputs with a varying linear ramp. An example of such numerical solutions is shown in Figure 5-10.

Risetime detection points out the fact that when a BOD is operating in the overshoot switching regime, its operation may depend on the transient properties of the incident light pulse, not just on the incident pulse energy. This fact must be taken into account in any system design.

Risetime detection, using overshoot switching, may be useful as an ultrashort pulse detector, which is described in the next section.

V.F Pulse Detection

The studies of overshoot switching utilized step-changes in input intensity. The studies of risetime detection involved linear ramps. In reality, most experiments using optical pulses will involve Gaussian-like pulses. We investigated overshoot switching and risetime detection with Gaussian input pulses. In addition, we considered the use of a cw holding intensity along with the pulses to provide a memory of the switching of the BOD. We found that this can, in principle, be used as an ultra-short pulse detector. This was discussed at CLEO (Garmire, Goldstone, Hendrix, CLEO, June 1981) and is being submitted for publication in Applied Optics.

Bistability means that a device can be used as a memory element. We have explored the use of this property to detect and record the existence of ultra-short pulses. This is of importance in the field of pico-second pulses. Consider, for example, a bistable device subject to a cw intensity sufficient to bias it to the bistable regime, and subject to an additional pulse (consider, for the moment, intensity addition for the two light beams). If the pulse is so short that the device does not have time to respond, the cw output will be in the low state. If, however, the pulse is long enough, the bistable device will switch to the higher state. Thus, the bistable · device acts as a detector for pulses whose lengths are longer
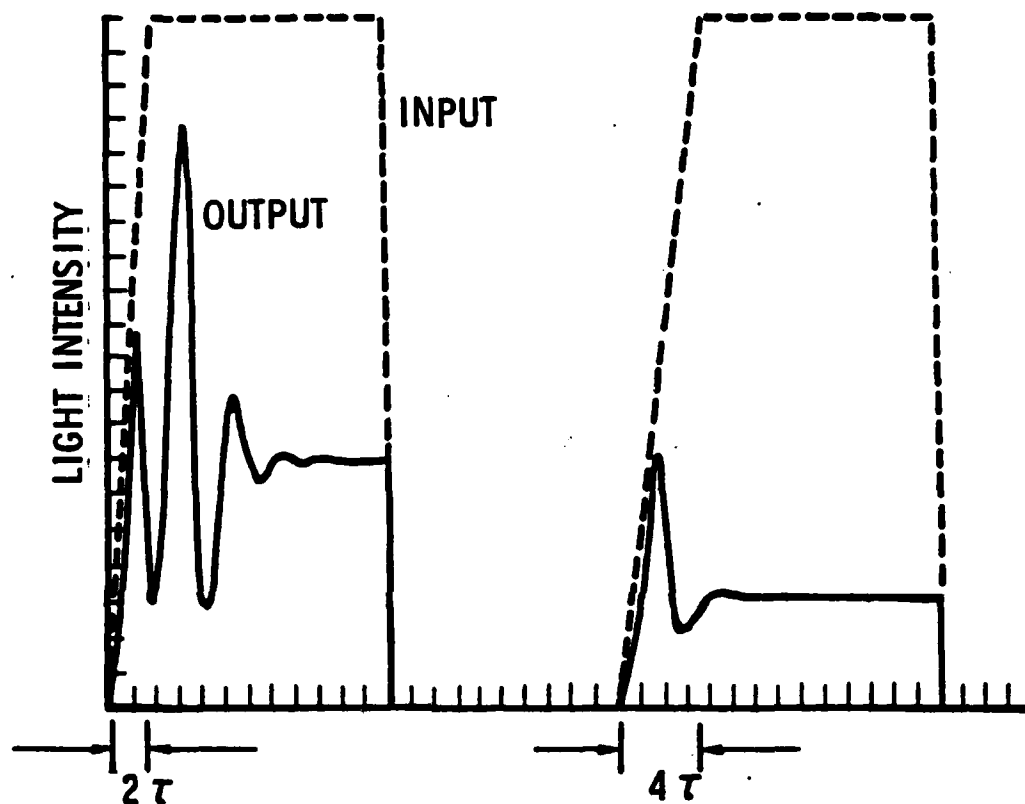
69

$$\tau_1 \cdot \tau_2 \equiv \tau$$

Figure 5-10. Risetime detection in overshoot switching. Bistable device will not switch unless the onset of the pulse is sufficiently fast. Results of numerical analysis of the nonlinear Fabry-Perot.

than the device response time. It does not switch when no
pulses are present or when the pulse is too slow.

In many applications it is desired to prove that a train
of pulses is faster than a certain value (since electronics can
detect slower pulses). In this case, we may use overshoot
switching to bracket the value of the pulse width. This is
shown in Figure 5-11. Here we show the use of the Gaussian
pulse in the overshoot switching regime superimposed on a cw
monitoring input. Notice that only for a particular Gaussian
pulsewidth does the device switch to its highest state. If
the pulsewidth is slower or faster than this value, the
device does not switch to the highest state.

Figure 5-11d is the transfer curve for the NLFP which gave
rise to the numerical simulations in the figure. Note that the
device is tristable. It can be seen that the holding intensity
must be within the multi-stable region, and the pulse height
must be within the overshoot switching regime. In this example,
we have chosen an input Gaussian sufficient to cause the device
to pass to its third stable state. The use of multistability
has the advantage that the presence of both long and short
pulses are still detected as a switch to the intermediate state,
leaving the BOD in a different state than if no pulse at all
had been present.

Of course, pulse detection, as described here, depends on
the incident light intensity which can be determined indepen-
dently by an energy measurement. In Figure 5-12 we show the
range of pulse widths which will cause the BOD to switch as a
function of the peak intensity of the device. Switching
occurs for any pulses within the cross-hatched region. It can
be seen that pulses which are too short will cause no switching
at all, and pulses that are very long will always cause
switching if the intensity is above the value of steady-
switching. The requirements to obtain a definitive value for
the pulse width are to operate within the overshoot switching
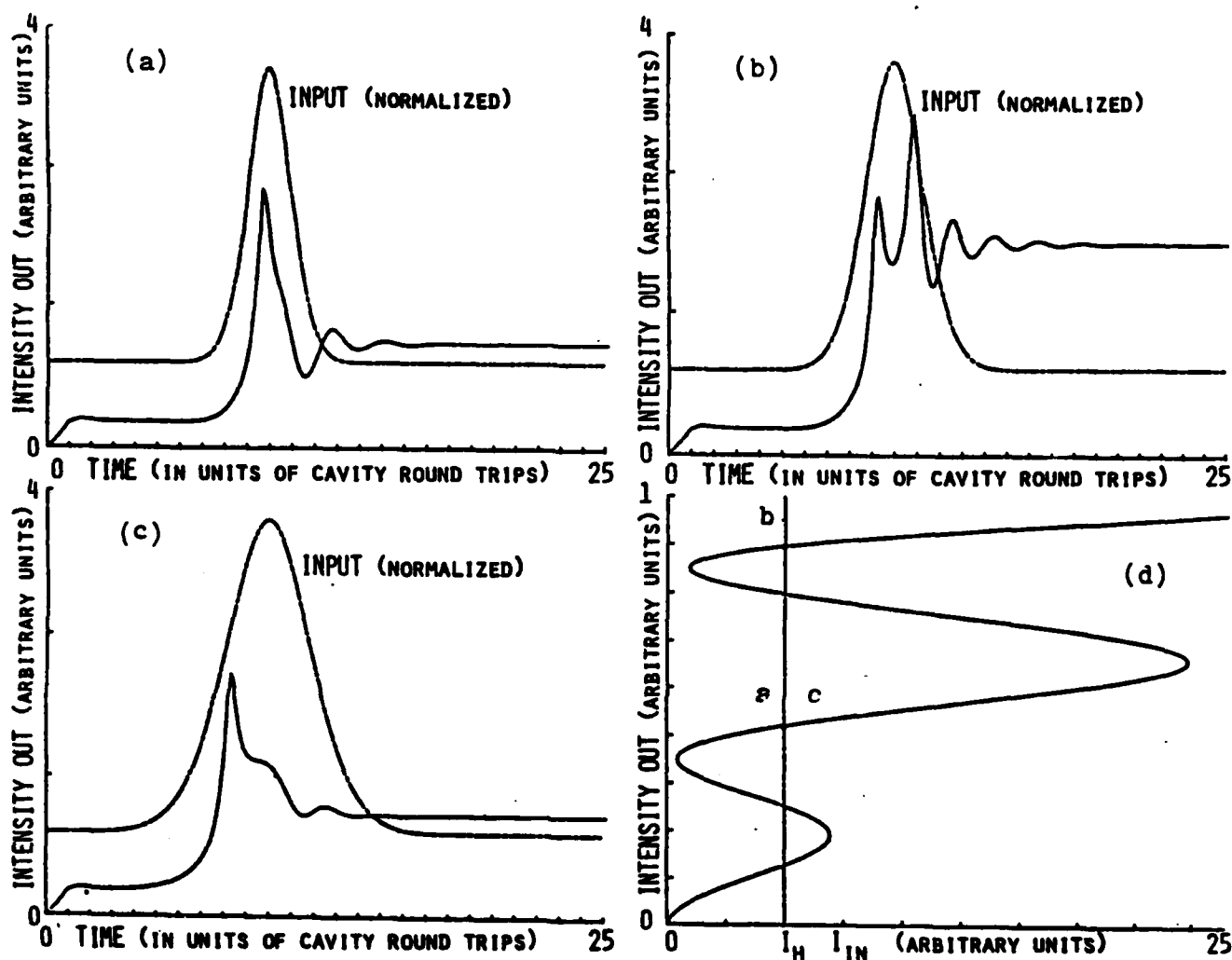regime, the "nose" in the figure. These calculations were

71

Figure 5-11. Use of bistable device in the overshoot switching regime as a pulse detector: (a-c) Output as a function of time for three different incident Gaussian pulsewidths, superimposed on a cw background within the overshooot switching regime. Notice that the output switches to the higher state only for a particular Gaussian pulsewidth. (d) Steady-state transfer curve (output intensity as a function of input intensity). I_H is the cw holding intensity. Letters indicate final holding intensities in each of the three figures.
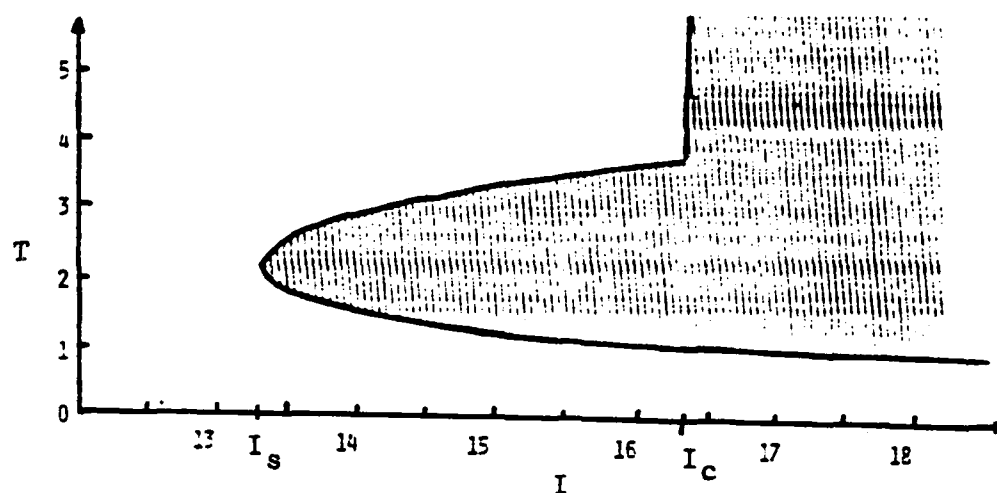
Figure 5-12.   Pulsewidth which causes
overshoot switching (in units of cavity response time) as a func-
tion of the peak incident.   The region which is cross-hatched
will cause switching of the BOD to the higher state.

made assuming the round-trip time in the cavity was equal to the response time of the nonlinear medium. Under these conditions, we detect pulses whose width is approximately twice that of the response time.

We saw from Figure 5-11 that the final cw state depended on the pulse length. If we consider a highly multistable device, we can obtain an output whose intensity level is proportional to the pulsewidth. We investigated this numerically, and obtained results such as those shown in Figure 5-13, in which both the cw holding intensity and peak pulse intensity were held constant, but the pulsewidth was allowed to vary. Differing output levels are obtained depending on the pulse width.

The output level depends, of course, also on the peak intensity. Figure 5-14 shows how the output intensity level depends also on intensity. In order to use the bistable device as a calibrated pulsewidth detector, it will be necessary to have an independent measure of the pulse energy, from which the peak intensity can be extracted.

In addition to adding <u>intensities</u> between the cw and pulsed light fields, we considered adding <u>fields</u>. Under these conditions, we found that there were conditions under which the two fields added out of phase, but with equal intensities, causing the field inside the device to go to zero, and therefore switching it off. The result of these investigation was the realization that the NLFP must be constructed so that <u>intensities</u> add.

V.G Self-Oscillation

We have discovered that under some conditions, "stable" states of the NLFP are, in fact, unstable and that the instabilities lead to self-oscillations. The results were presented at the Optical Society of America (Goldstone and Garmire, Opt. Soc. Am., Florida, 1981). and are being submitted to the Journal of Quantum Electronics. Our considerations are for the NLFP in which the medium response time is longer than the cavity response time. This is the opposite regime from the "chaos" regime.
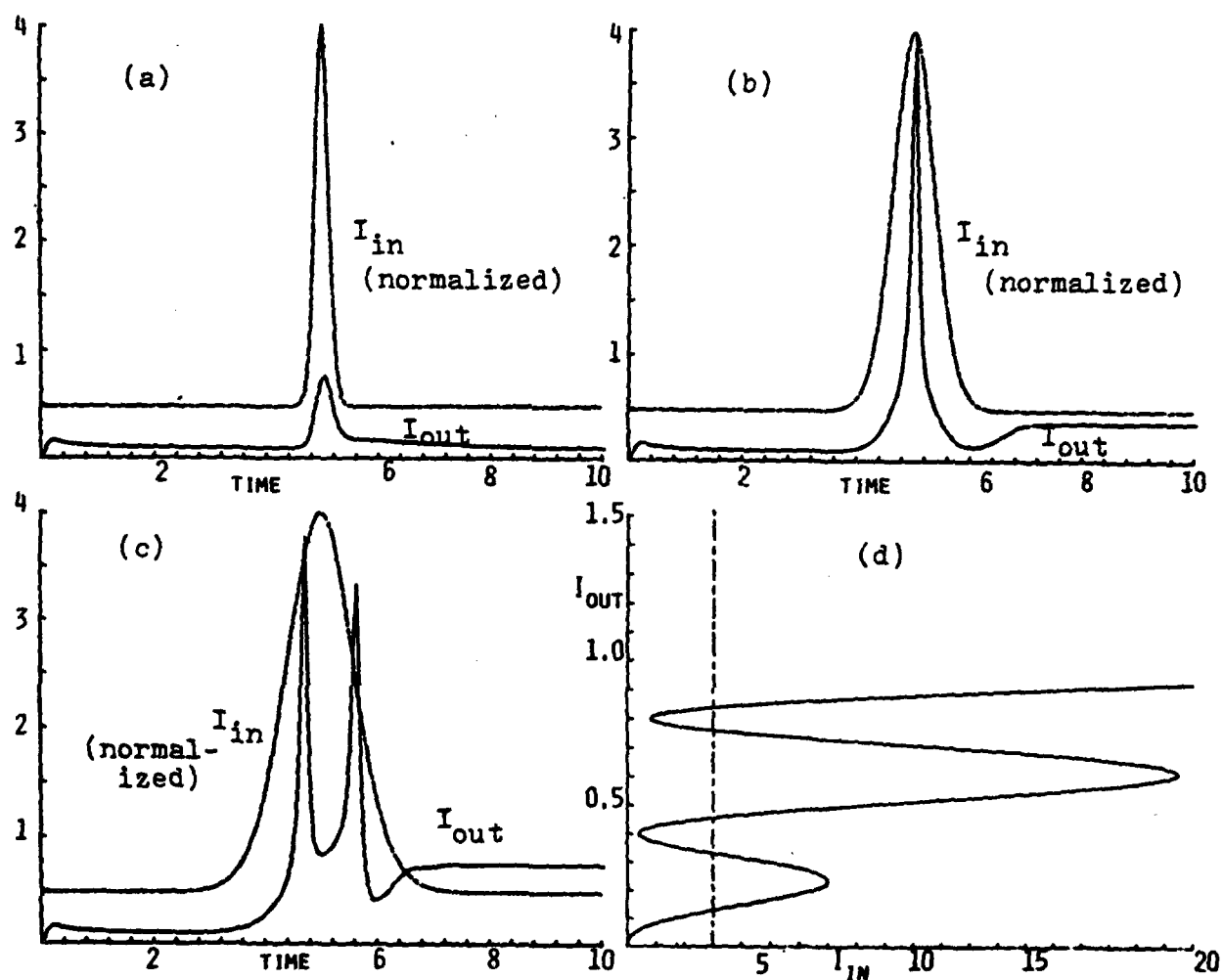
74

Figure 5-13. Response of a multi-stable nonlinear Fabry-Perot to a Guassian pulse superimposed on a cw holding intensity: (a-c) Output as a function of time for three different pulsewidths. Notice that three different output holding intensities result from three different pulsewidths. (d) Steady-state transfer curve. Holding intensity is marked by vertical line.
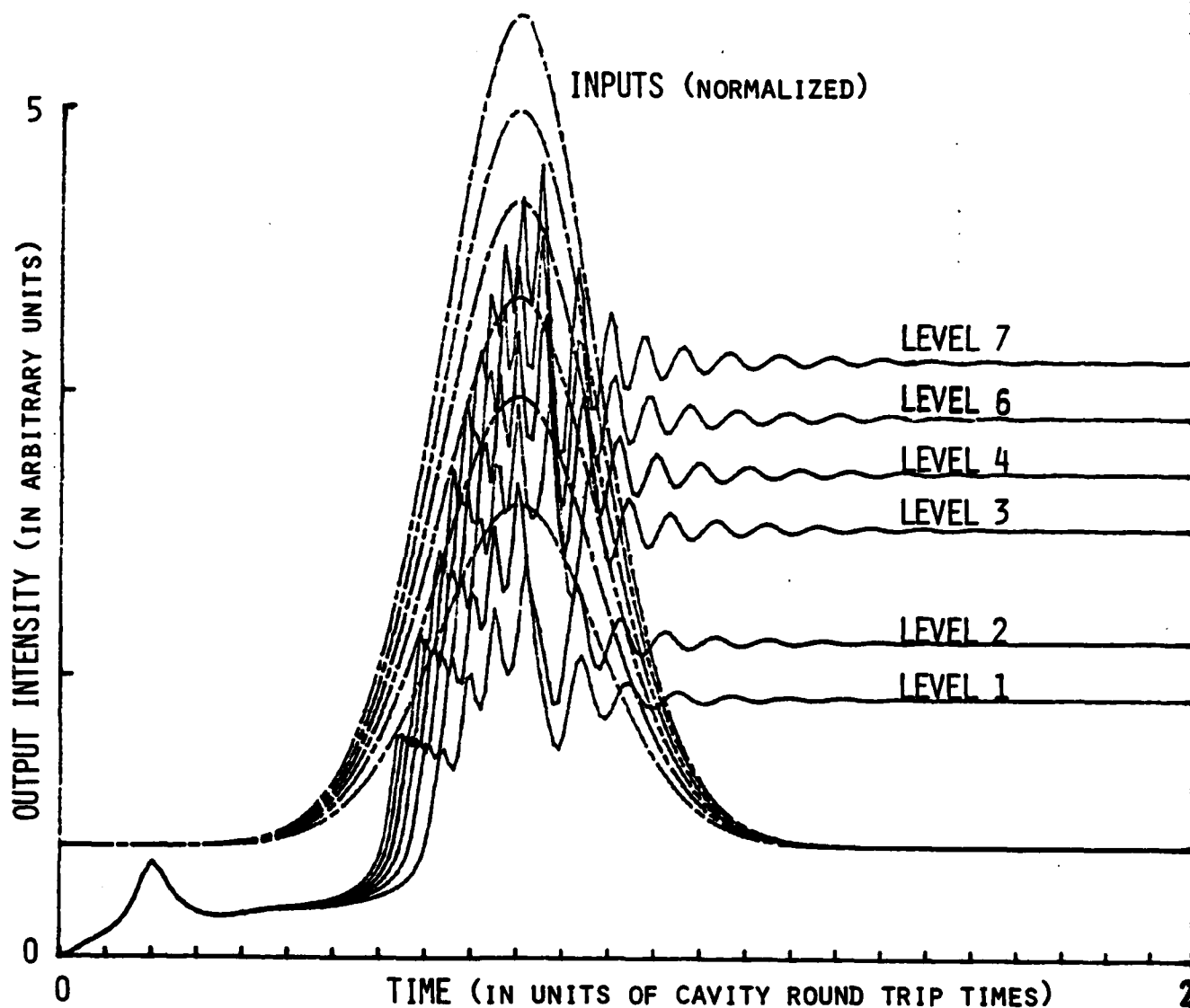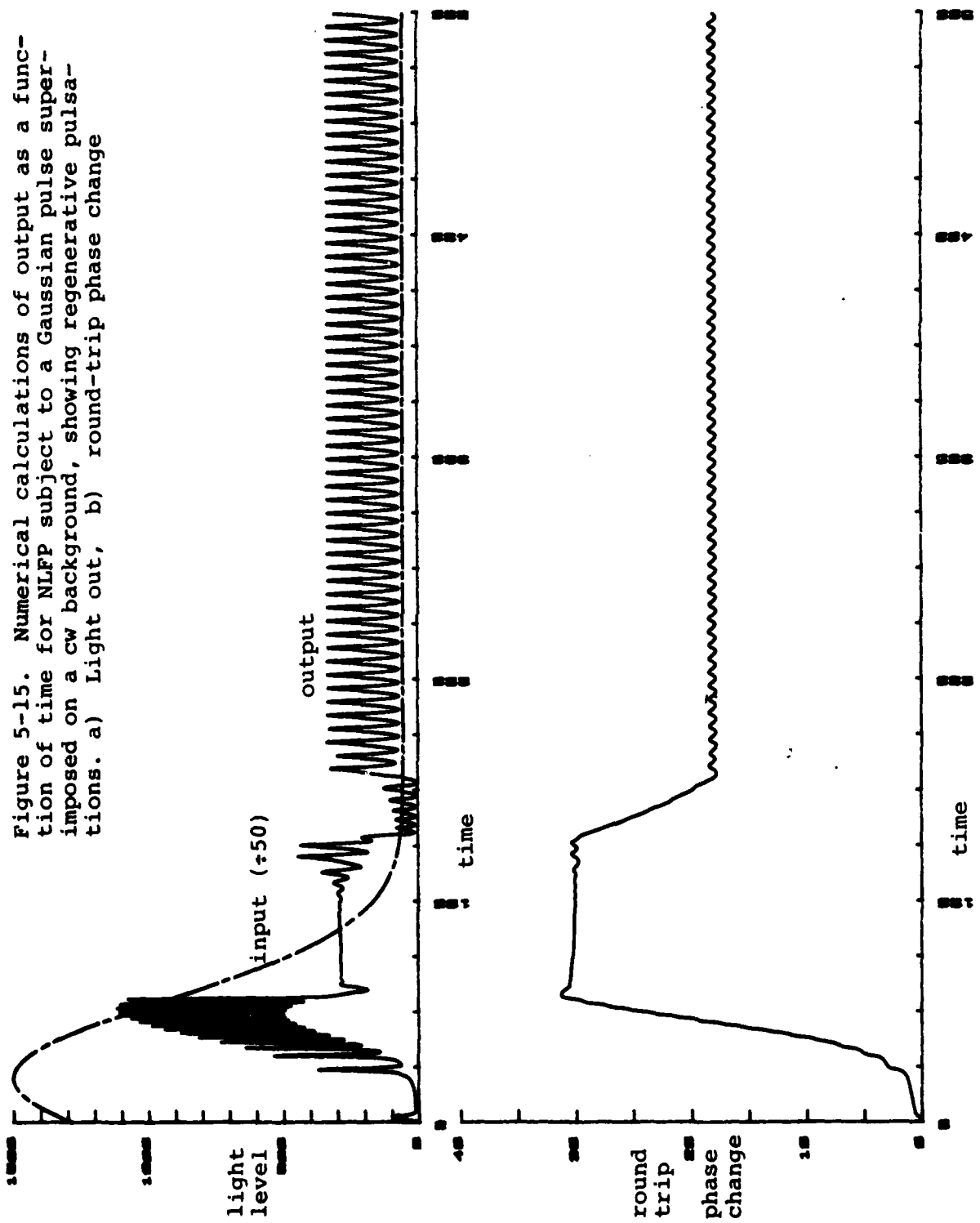
Figure 5-14. Output as a function of time for Gaussian pulses of varying heights, for fixed pulsewidths and cw input. Inputs are shown as dotted lines.

The instabilities reside predominantly on the upper branches, although it is possible to obtain instabilities on lower branches if the finesse is very high. The instabilities occur when the medium response time is as much as 1000 times the round-trip time, but do not occur when the round-trip time is truly negligible. However, the largest regions of instability occur when the response time is about ten times the cavity round-trip time.

By analyzing our analytic approximations, we have shown that instabilities occur on the lower branch only when the finesse is very high (reflectivities ~0.99). As one considers higher branches in a multi-stable system, the region in input intensity over which instabilities are observed becomes wider, the effect being more pronounced for higher finesse. Typically, a region of about 5% of the incident intensity is unstable for the second branch and reflectivity of 0.9. If the device operates on the seventh or eighth branch, reflectivities as low as 70% can have wide regions of instabilities which cause self-oscillation. In the relatively lossy systems which appear to be most useful for optical signal processing in a thin NLFP, finesses will be low, and self-oscillation will probably not be a problem, for the first few levels.

The instabilities occur typically near cavity resonances, and result in self-oscillations with a period of between 10 and 100 cavity round trips on the lower branches and down to only a few roundtrips on higher branches. The faster the oscillations, the smaller their amplitude.

In addition to an analytic understanding of these oscillations, we have obtained numerical solutions of equations 5-4 and 5-5 which demonstrate the oscillations, and obtained good agreement between the analytic approximations and the numerical solutions. Figure 5-15 shows one computer result, using a Gaussian pulse input leading to a cw input. In addition to the output intensity, the round-trip phase change is shown,

77

Figure 5-15. Numerical calculations of output as a function of time for NLFP subject to a Gaussian pulse superimposed on a cw background, showing regenerative pulsations. a) Light out, b) round-trip phase change

indicating the origin of the self-oscillations. Notice that the peaks which occur from the device passing through its transmission peaks do not cause oscillations in the phase. However, as a quasi-steady-state output begins to occur on a relatively high level, an oscillation in phase begins to build up, until the oscillation has sufficient amplitude to cause the device to down-switch several levels to a lower state. This lower state never reaches a constant value but oscillates continuously in a regenerative fashion. Notice that the larger amplitude output pulsations occur from a small fractional modulation of the round-trip phase change.

We feel we now have a good understanding of the dynamic response of the nonlinear Fabry-Perot under the conditions that the medium response time is equal to or longer than the cavity round-trip time. This is the regime of greatest interest for image processing, in which ultra-thin nonlinear Fabry-Perots will be used. In the last section we look at self-oscillations which occur when a three-mirror Fabry-Perot is used.

V.H Three-Mirror Pulser

We have shown that self-oscillations occur in the NLFP under conditions of high finesse. It is also possible to create self-oscillations by introducing a third mirror some distance away from a nonlinear Fabry-Perot. Since this is relatively easy to do experimentally, it is suggested that the three-mirror pulser may be more convenient than using self-oscillations, if a bistable device is to be used to create a train of pulses from a cw optical signal.

We obtained a set of equations for the dynamic response of a set of two coupled cavities. The system will pulse when the round trip time of the first (linear) cavity is long compared to the response time of the medium and round-trip time in the (second) NLFP . The additional feedback from the additional mirror causes the NLFP to self-pulse.

The pulsation rate depends on the input intensity, as well as the bias phase. A typical result is shown in

79

Fig. 5-16. Note that, in addition to the relatively wide pulses created by the third mirror, the system gives a sharp peak every time the transmission of the NLFP goes through a maximum.

It is beyond the scope of this report to describe this study in detail. It is more fully described in a recent publication (Goldstone and Garmire, IEEE J. Quantum Electr. QE-17 372 (1981)).
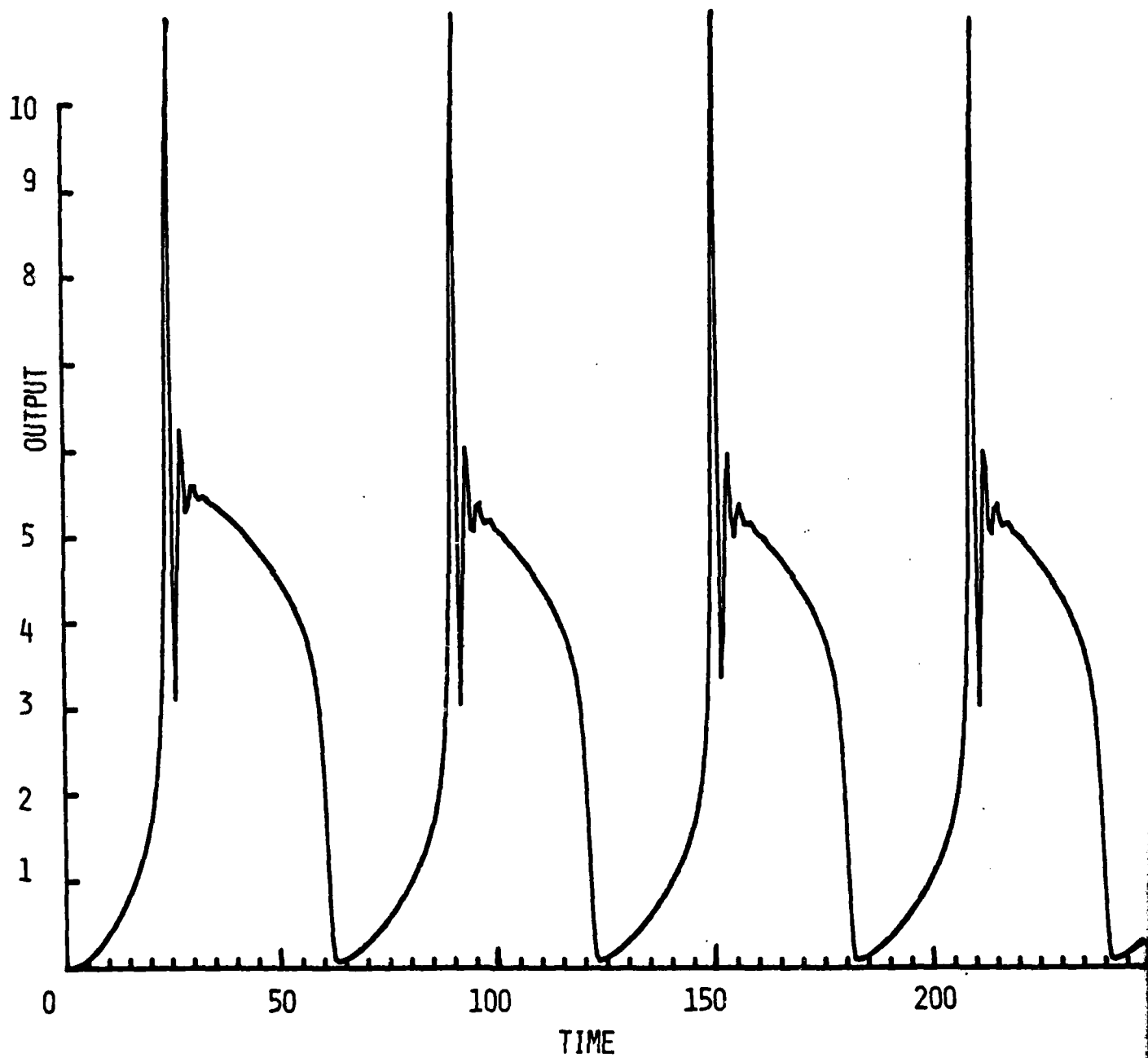
Figure 5-16. Self-pulsing in a nonlinear cavity with three mirrors. The nonlinear medium is assumed to be contained between two of the mirrors.

81

DATE
ILME
—8